Chromium – Copper – Iron

Tamara Velikanova, Mikhail Turchanin

Introduction

Phase equilibria in the Cr-Cu-Fe alloys are of importance both for the development of Cr-Cu-Fe alloys and for their possible use in recycling processes in metallurgy. The Cr-Cu-Fe system is of interest for ferrous and nonferrous metallurgy and for development of Cu based composites with favorable mechanical and electrical properties. The Cu rich alloys of the system are promising as new cost effective, high strength, high conductivity copper alloys. Copper has widely been used as an alloying element in ferrous metallurgy to improve strength of steels under aging, their corrosion resistance and antifriction properties. On the other hand, the presence of copper in ferrous alloys has negative aspects as well. It is known that a small amount of residual Cu in steel scrap, which is difficult to remove by conventional steelmaking process, is a reason of "surface fissures" during hot rolling process. The solubility of Cu in solid Fe, and therefore the influence of Cr on the solubility, and liquid-solid wettability are considered as important factors affecting surface fissures formation. Features of phase relations in the Cr-Cu-Fe alloys appeared to help solving the problem of Cu separation from steel scrap, which is important for both metallurgical processing difficulties and environmental problems. All these aspects stimulated intensive investigation of the Cr-Cu-Fe alloy phase diagram. The main works are listed in Table 1.

Seven temperature-composition sections in the Fe rich corner of the diagram, three at constant chromium and four at constant copper content, were reported by [1939Mor]. It is worth noting that the alloys investigated below the solidus were contaminated with carbon up to 0.1 mass%. Additional information on vertical sections at 2 and 4 mass% Cu in a high Fe content composition range was reported by [1970Ahm, 1974Zap] on alloys obtained by powder-metallurgical process and later the sections were calculated by [1998Mie]. The calculated temperature-composition sections at 1 and 4 mass% Cu in the whole concentration range were reported by [2004Wan] on the basis of own experimental data. The phase equilibria were studied in a wide composition range, and a number of isothermal sections were constructed in the temperature range from 800 to 1300°C by [1967Sal, 1993Hao, 1997Oht, 2001Fer1, 2002Wan]. The effect of Cr on the solubility of Cu in iron was investigated by [1967Sal] using alloys based on mild steel. All the available experimental data on the phase equilibria in the ternary Cr-Cu-Fe system generally well agree. Miscibility gap in liquid of the system was studied by [2004Wan].

The results of investigations of physical, chemical and mechanical properties of Cr-Cu-Fe alloys obtained by both conventional and powder metallurgical methods were presented by [1967Sal, 1970Ahm, 1974Zap, 1971Yam, 2001Les, 2001Fer1, 2001Fer2, 2001Fer3, 2001Son, 2002Kim].

The Cr-Cu-Fe system was first critically assessed by [1979Cha]. This assessment was mainly based on the results of [1939Mor, 1970Ahm, 1974Zap]. The same data set was used for modeling thermodynamic properties of (Cu), α and γ phases of the system in the framework of development of approximate thermodynamic solution phase data for steels [1998Mie]. The thermodynamic parameters of the ternary system were evaluated by [1997Oht] on the basis of own experimental results for the solubility ranges of phases in the temperature interval 1100-1300°C, and an isothermal section of the system at 1200°C was presented. The thermodynamic assessment of the phase equilibria in the Cr-Cu-Fe system was carried out by [2002Wan] on the base of own experimental results and data of [1997Oht] taking into account data of previous works, excluding [1967Sal] who investigated the Cr-Cu-mild steel alloys instead of Cr-Cu-Fe as mentioned above. The results of calculation agree well enough with the experimental data available. The optimized and consistent thermodynamic description of the Cr-Cu-Fe system of [2002Wan] was used for calculation of the majority of figures on phase relations and reaction scheme presented in this assessment.

Binary Systems

The assessments of the Cr-Fe system by [1987And], of the Cr-Cu system by [1990Ham] and of the Cu-Fe system by [1995Che] are accepted. These works are in good consent with [2002Ans, 2006Tur, Mas2]. The

thermodynamic data sets of [1987And, 1990Ham, 1995Che] were used by [2002Wan] for thermodynamic assessment of the ternary Cr-Cu-Fe system.

Solid Phases

Table 2 summarizes the crystallographic data on the Cr-Cu-Fe phases and their temperature and concentration ranges of stability. The (Cu), α and γ phases have marked homogeneity ranges in the ternary system.

Cr and Fe decrease the solubility of each other in (Cu). The solubility of Cr in the (Cu) phase is not significantly decreased by addition up to 0.3 mass% Fe after [2001Fer]. The solubility of Fe in the (Cu) phase is significantly reduced due to the presence of Cr. At 750°C and below this tendency becomes less brightly expressed. This indicates that at lower aging temperatures less precipitation occurs during sample quenching.

An increase in the Cr solubility in the γ phase with increasing Cu concentration and a decrease in the Cu solubility in the γ phase with increasing Cr concentration was found by [1939Mor, 1967Sal, 1970Ahm, 1974Zap, 1993Hao, 1997Oht, 2002Wan] to be general tendencies. The minimum of Cu solubility in austenite of mild steel with 5-7 mass% Cr reached in equilibrium with liquid at 1250°C was reported by [1967Sal]. It was not confirmed by the experimental investigations of [1993Hao, 1997Oht, 2002Wan] and the thermodynamic calculations of [1997Oht, 2002Wan] for the ternary Cr-Cu-Fe alloys. According to our calculation based on the thermodynamic models of [2002Wan], the γ phase homogeneity range penetrates down to ~80 at.% Fe at 1100 to 1300°C in the ternary system.

The calculated maximal saturation of the α phase by copper is about 8 at.% Cu at 1380°C. This value correlates well with the experimental results of [1993Hao, 1997Oht].

The (Cu), α and γ phases were treated as ternary solid solution phases in the thermodynamic assessment of [2002Wan]. For the σ phase the homogeneity range only in the binary system was taken into account in the calculation.

Invariant Equilibria

The data on the invariant equilibria given in Table 3 follow from the thermodynamic calculation carried out in the present assessment. The reaction scheme after the calculation is given in Fig. 1. The existence of the miscibility gap of the liquid phase in the ternary system despite its absence in the boundary binary systems is an interesting peculiarity of the ternary. The existence of the point corresponding to the cupola top of the miscibility gap of liquid, c_1, and of two critical invariant points, c_2 and c_3, corresponding to the origin of the three-phase monovariant equilibria of the α and γ phases with two liquid phases rich in Fe or Cu given in Table 3, reflects such a specific interaction of the components in the ternary. Invariant four-phase monotectic equilibrium of the transition type, U_1, and invariant equilibrium of the transition type, U_2, are shown. The calculated temperature of the U_2 equilibrium, 1088°C, agrees perfectly with that measured experimentally by [1939Mor], 1084°C. The calculated and experimental compositions of the α and γ phases are also close.

Liquidus and Solidus Surfaces

A liquidus projection is given in Fig. 2a (in the whole composition range) and in Fig. 2b (enlarged part near the Cu corner) according to the thermodynamic calculation performed in this assessment. A wide two-phase L' + L" region exists in the ternary system over a large composition range. Addition of Cr to the Cu-Fe alloys decreases the liquidus temperature of the γ phase as well as addition of Fe to the Cr-Cu alloys decreases the liquidus of Cr-Cu alloys (liquidus of α-phase) down to the monotectic valleys L' ⇌ L" + γ and L' ⇌ L" + α, respectively. The above mentioned feature gives rise to the minimum fold on the liquidus surface of the α phase in the ternary system. The fold extends from the point of the temperature minimum in the solid-liquid equilibrium region of the binary Cr-Fe up to the invariant e_1(min) point at the monovariant monotectic L' ⇌ L" + α line in the ternary system. Accordingly, the tie lines L'L" in the equilibria L' + L" + α, which radiate from the Cu corner torwards the Cr-Fe side, go from the c_2 and c_3 critical points to meet

one another at the minimal temperature on the ruled surface L'L" at 1362°C. The composition range of the primary crystallisation surface of (Cu) is shown to be very restricted in agreement with the data for the binary Cr-Cu and Cu-Fe phase diagrams.
The calculated solidus surface projection is given in Fig. 3. The narrow γ + α + (Cu) three-phase region shifted to the Cu-Fe edge separates the two-phase γ + (Cu) and α + (Cu) regions. A very slight decrease in solidus temperature from the Cu-Fe to Cr-Cu boundary systems is observed. According to the calculation, the solubility of Cu in the (αFe) and (γFe) phases at solidus decreases from 5.8 and 6.9 at.% in the binary Cu-Fe after [2006Tur] down to 3.9 at 18.3 at.% Cr and 5.7 at.% at 14.7 at.% Cr at 1088°C, respectively. The content of Cr in (Cu) solid solution is rather small being of 0.3 at.% at 3.4 at.% Fe.

Miscibility Gap Surface

The calculated miscibility gap of the liquid phase in the ternary system in the stable and metastable ranges is given in Fig. 4. The isotherms at 1127 to 1477°C are taken from [2004Wan]. The set of the vertical sections of the miscibility gap parallel to the Cu-Fe edge is given in Fig. 5. The curve at 4 mass% Cr is taken from [2004Wan]. The others are shown after the present calculation. Figures 4 and 5 show that additions of Cr to Cu-Fe alloys and Fe to Cr-Cu increase the critical temperature of the miscibility gap (metastable in the binaries Cu-Fe and Cr-Cu). Above 1.7 at.% Cr addition to Cu-Fe (critical point c_3 at 1431°C) the stable miscibility gap appears. The minimal addition of Fe to Cr-Cu alloys to stabilize the miscibility gap is 9.7 at.% (critical point c_2 at 1516°C). One can see that the stable miscibility gap exists in a wide composition region in the ternary system, forming the rather flat cupola with maximum at 1523°C.

Isothermal Sections

Isothermal sections at 1500, 1250, 1050, and 800°C are given in Figs. 6 to 9 according to the thermodynamic calculations. The calculated isothermal sections at 1000, 1100 and 1300°C were reported by [2002Wan]. Additionally the isothermal sections at 1600, 1500, 1400, 1250, 1200, 1050, 900 and 800°C were calculated in the present assessment using the thermodynamic models of [2002Wan]. The results of the calculations correlate well with the experimental investigations of [1993Hao, 1997Oht, 2001Fer1, 2002Wan].
No experimental data on phase equilibria at temperatures above 1300°C are published. Strong bend of the L / L + α boundary towards the Cr-Fe edge giving a minimum Cu content at about 20 at.% Fe is seen in the calculated section at 1500°C, Fig. 6. This feature agrees with the location of the invariant minimum at 1513°C and 21 at.% Cr in the boundary Cr-Fe system.
The composition of the equilibrium phases (Cu) / (αFe) at 800°C, (Cu) / (γFe) at 900, 1000°C and L /(γFe) at 1200°C were reported by [2002Wan] for the Fe rich alloys of the Cr-Cu-Fe system. The alloys were prepared by melting and subsequently hot-rolled at 900°C, solution-treated at 900°C for 24 h, heat-treated at 800 to 1000°C for 336-1680 h and then quenched in iced water. It was tested and confirmed that the specimens had reached an equilibrium state. The equilibrium compositions were determined up to a Cr content of 10.1, 10.79, 10.85 mass% in the Fe based phases and 0.22, 0.21, 0.49 mass% in the (Cu) phase at 800, 900 and 1000°C, respectively. The (γFe) solid solution of the composition 9.20Cr-3.38Cu (mass%) was found to be in equilibrium with liquid of the composition of 0.12Cr-97.77Cu (mass%). The equilibrium compositions of the solid and liquid phases at 1100, 1200 and 1300°C were measured by [1997Oht] using solid-liquid diffusion couples held at the above mentioned temperatures for 24-48 h and subsequently quenched in iced brine. The average composition of the frozen solid and liquid at the interphase boundaries of the diffusion couples were obtained up to a Cr content of 28.81, 15.33, 16.40 mass% in solid and of 0.52, 0.47, and 0.80 mass% in liquid at 1100, 1200 and 1300°C, respectively. It was shown that the addition of Cr decreases the solubility of Cu in the Fe based phases. This tendency becomes remarkable with increasing temperature. Being obtained using diffusion couples technique the experimental data of [1997Oht] might be less reliable than those of [2002Wan] who used conventional metallurgical methods and well equilibrated alloys. However, the data of both [1997Oht] and [2002Wan] perfectly agree, and good agreement was achieved between the calculated locations of the phase boundaries and the experimental results. The isotermal sections at 1200°C constructed by [1997Oht] is cited in the review by [2002Rag].

The Cr effect on the solubility of Cu in austenite of mild steel at 900, 1100 and 1250°C was studied by [1967Sal]. The measured solubility of Cu in Fe based phases is slightly lower compared with the results of [1997Oht, 2002Wan], and a slight minimum of the solubility upon addition of about 5-6 mass% Cr was found. The minimum point of Cu solubility in Fe based solid solution, reported by [1967Sal], was not confirmed by the calculation for the Cr-Cu-Fe system.
The calculated sections at 1300, 1250,1200 and 1100°C demonstrate the equilibria of the α, γ and liquid (very rich in Cu) phases and differ from each other in the equilibrium compositions of phases only. The phase equilibria at 1250°C are shown in Fig. 7. The equilibrium composition of phases at this and the above mentioned temperatures are given in Table 4. The calculated isothermal section at 1050°C is given in Fig. 8. The same feature of the phase equilibria formed by α, γ and (Cu) phases is shown in the calculated isothermal sections at 1000 and 900°C. Only the compositions of equilibrium phases differ. They are given in Table 5. The isothermal section at 1000°C, reported by [1993Hao], shows slightly elevated Cu content in the α and γ phases in equilibrium with (Cu) phase comparing with the data of [2002Wan]. [1993Hao] based on own study of three ternary diffusion couples annealed for 150 h with subsequent quenching in water. The (Cu) / (Cu) + α boundary at 1050°C after the calculation is shown in Fig. 8. It agrees well with the experimental results of [2001Fer1] obtained using WDS method. One can see in Fig. 8, that Fe decreases the solubility of Cr in (Cu) at 1050°C, and the solubility of Cr reduces more markedly with increasing Fe content. Similar tendency was found by [2001Fer1] for lower temperatures (down to 500°C) using resistivity measurements on aged and subsequently quenched in water alloys. However, the values of the solubility measured by this method at 1050°C were found to be noticeably lower than those after WDS method. Consequently, the isotherms at 1025, 1000, 950, 850, 750, 650 and 500°C reported by [2001Fer1] cannot be considered for description of the equilibria at the indicated temperatures.
The calculated isothermal section at 800°C is shown in Fig. 9. The (Cu) + (αFe) / (αFe) phase boundary shown in Fig. 9 agrees with that of [2002Wan] obtained up to about 10 mass% Cr. There are no experimental data on a possible Cu solubility in the σ phase. It is assumed to be small taking into account the size of the Cu atomic radii on one hand, and Cr and Fe radii, on the other hand. Isothermal sections in the temperature interval 831 to 510°C, where the σ phase is stable in the Cr-Fe binary system, have to differ in the σ + (Cu) and neighboring α + (Cu) + σ regions only.

Temperature – Composition Sections

The calculated vertical sections are shown in Figs. 10 to 24. The section at 1 mass% Cr is taken from [2004Wan], and the others are given after the calculation performed in the present assessment corresponding to [2002Wan, 2004Wan]. Satisfactory agreement of the published calculations [1997Oht, 2002Wan, 2004Wan] in a wide temperature range including the region of the equilibria with liquid phase and the available experimental data of [1939Mor, 1970Ahm, 1974Zap, 1997Oht, 2002Wan, 2004Wan] was achieved as mentioned above. Thus one should believe that the thermodynamic models evaluated by [1997Oht, 2002Wan] fit well to the thermodynamic description of the vertical sections in the whole composition range at the temperatures under consideration, and the calculated vertical sections are reliable.
The first detailed experimental investigation of the temperature-composition sections of the Cr-Cu-Fe system was carried by [1939Mor]. Contamination with 0.04 to 0.11 mass% carbon was reported for the alloys used in the study of phase equilibria in the solid state. Seven partial vertical sections for the Fe rich part of the system were presented: at 2 mass% Cr (up to about 20 mass% Cu), at 5 and 14 mass% Cr (up to 40 mass% Cu), and at 1, 2, 4 and 5 mass% Cu (up to 20 mass% Cr). The results of the later works of [1970Ahm, 1974Zap, 1993Hao, 1997Oht, 2002Wan] concerning the mutual solubility of Cr and Cu in the γ phase and the solidus temperatures generally agree with the presented vertical sections. [1939Mor] found that the γ phase homogeneity range is enlarged by addition of copper so that the γ/γ + α boundary lies between 14 mass% Cr at 5 mass% Cu and 19 mass% Cr at 4 mass% Cu at about 1084°C. With increasing Cr content, the solubility of Cu in the γ phase and the Cu content at eutectoid composition at first decrease and then increase, while the eutectoid temperature changes slighly. [1970Ahm, 1974Zap] studied the influence of Cr on phase relations in the Fe rich alloys along the sections at 2 and 4 mass% Cu up to 18 and 15 mass% Cr in the temperature range from the solidus down to 700 and 1100°C, respectively.

The calculated vertical sections at 2 and 5 mass% Cr given in Figs. 11 and 13, at 1 and 4 mass% Cr [2004Wan] given in Figs. 10 and 12, as well as at 1, 2, 4 and 6 mass% Cu, Figs. 18 to 21, confirm the above mentioned a peculiarity of the ternary system, namely, the widening of the γ phase homogeneity range in the equilibria with the α phase when Cu is added. The miscibility gap of the liquid phase is shown in the sections parallel to the Cu-Fe edge at 2 mass% Cr and more (including the highest content of Cr up to 40 at.%), Figs. 11 to 17. The same is seen in the sections parallel to the Cr-Fe edge at 2 mass% Cu and more given in Figs. 19 to 22. The isothermal line at 1395.5°C, corresponding to the monotectic invariant equilibrium U_1, appears in the sections at 4 and 5 mass% Cr as well as at 20 at.% Cu additionally to the L' + L" region, as shown in Figs. 12, 13 and 22a, 22b. The isothermal plane of the invariant four-phase equilibria corresponding to the α + γ + (Cu) three-phase alloys solidification is intersected by the vertical sections at 1, 2, 4, 5 and 14 mass% Cr, Figs. 10 to 14.
The minimum on the liquidus surface in the sections at 1, 2, 4 and 6 mass% Cu, Figs. 18, 19a, 20 and 21, near 20 at.% Cr at the temperature close to 1500°C is associated with the invariant minimum on the liquidus/solidus of the Cr-Fe binary system at 21 at.% Cu and 1513°C.
The very narrow L' + L" + α and L' + L" + γ ranges spearing the L + α and L + γ fields, respectively, as shown in the sections at 2, 4 and 6 mass% Cu, Figs. 19a, 20 and 21, seem to be very unusual. At higher Cu content, a minimum at 1362°C within the curves separating the L' + L", L' + L" + α and L + α phase regions appears, Figs. 22a, b. It corresponds to the intersection of the degenerated into the line L' + L" + α tie triangle with the plane of this vertical section.

Thermodynamics

There are no experimental data about thermodynamic properties of ternary solution phases in the system. In [1974Sig] and [1988Uen] the thermodynamic properties of liquid alloys in the ternary system were modeled on the basis of theoretical ideas and equations for interaction parameters in ternary solution were developed. In [1997Oht, 1998Mie, 2002Wan] thermodynamic properties of the ternary solution phases, L, (Cu), α and γ, were modeled on the base of data on phase equilibria between these phases. All the results of the calculation, both theoretical modeling and thermodynamic optimization of phase equilibria, demonstrate strong positive deviations of the thermodynamic properties of the solution phases from the ideality. In all cases when ternary interaction parameters were taken into account they have highly positive values. Thus, positive deviations from the ideality, inherent in phases of the boundary Cr-Cu and Cu-Fe binary systems, become more significant in the ternary. As a result, the miscibility gap in the liquid phase, which is metastable in the binary Cr-Cu and Cu-Fe melts, appears in the ternary system.
The thermodynamic assessment of the Cr-Cu-Fe system was carried out by [2002Wan] using the CALPHAD approach. Binary interaction parameters for the Cr-Cu, Cr-Fe and Cu-Fe systems were taken from previous works of [1987And, 1990Ham, 1995Che]. Thermodynamic descriptions for the liquid, (Cu) and γ phases were taken from [1997Oht]. Thermodynamic description for the α phase was obtained by [2002Wan] on the basis of the experimental data of [1997Oht, 2002Wan]. The ternary parameter for liquid phase was equal to zero. The excess thermodynamic properties of solid solution phases took into account the mixing enthalpy and the mixing entropy of components.
Due to the lack of experimental information, the solubility of σ phase in the ternary system is not considered in [2002Wan]. The thermodynamic assessment was carried out for temperatures above 900°C.

Notes on Materials Properties and Applications

The experimental works devoted to study of materials properties in the Cr-Cu-Fe system are listed in Table 6.
New cost effective, high-strength, high-conductivity and resistant to softening copper rich Cr-Cu-Fe alloys were developed and their properties were investigated by [2001Fer1, 2001Fer2, 2001Fer3]. Determination of the temperature dependence of the solid solubility of Fe and Cr in copper at 500 to 1050°C for alloys containing 0 to 1 mass% Cr and 0 to 1 mass% Fe was undertaken by [2001Fer1] to help interpreting the observed mechanical and electrical properties of alloys. The linear relationship between resistivity and chromium and iron concentrations in the Cu based solid solution was found by [2001Fer1]. Similarly, the

relationship between the resistivity and composition of alloys was also approximately linear after the solid solubility limit of (Cu) phase has been exceeded. Using these data the limit composition of (Cu) solid solution was determined in aged and subsequently quenched alloys.
The evident difference in the compositions of the (Cu) solid solution coexisting with α (or γ) phase was observed depending on experimental technique, namely WDS method or electrical resistivity measurements. The lower solubility observed by the resistivity measurements was explained by the partial (Cu) solid solution decomposition accompanied by small secondary precipitations under quenching experiments. The WDS method gives an average signal including concentration of the above mentioned precipitations. The method based on resistivity measurements gives only composition of (Cu) solid solution remaining under quenching. Thus the curves shown in Fig. 23 by thin lines are not isotherms of solubility at given temperatures. They correspond to unknown lower temperatures.
The mechanical properties of the Cu -0.7 mass% Cr - 0.3 mass% Fe alloy which indicated large precipitation hardening response combined with the ability to stabilize cold worked microstructures to high temperatures with a high electrical conductivity remaining were reported by [2001Fer2]. The age hardening response of the Cu - 0.7 mass% Cr - 2.0 mass% Fe alloy was minimal, but the resistance to softening was superior to that reported for any commercial high-strength, high-conductivity copper alloy with comparable mechanical and electrical properties. For example, an excess of 85% of the original hardness of the 40 % cold worked alloy is retained after holding at 700°C for 1 h, whereas commercial high-strength, high-conductivity Cu-Fe-P alloys have been reported to soften significantly after 1 h exposure below 500°C. The Cu - 0.7 mass% Cr - 2.0 mass% Fe alloy was expected to be more suitable for applications with a significant risk of exposure to elevated temperatures. Optical microscope examination of cold worked and aged microstructures confirmed the high resistance to recrystallization for Cu - 0.7 mass% Cr - 2.0 mass% Fe. The Zener-Smith drag term, predicting the pinning effect of second phase particles on dislocations in cold worked microstructures, was calculated using the precipitate characteristics obtained from TEM, WDS and resistivity measurements [2001Fer2, 2001Fer3]. The pinning effect of the precipitate dispersions in the peak-aged condition was determined to be essentially equivalent for the Cu - 0.7 mass% Cr - 0.3 mass% Fe and Cu - 0.7 mass% Cr - 2.0 mass% Fe alloys. A lower recrystallization temperature in the Cu - 0.7 mass% Cr - 0.3 mass% Fe alloy was therefore attributed to faster coarsening kinetics of the secondary precipitates resulting from a higher Cr concentration in the precipitates at a lower iron content [2001Fer3].
The microstructure and mechanical properties of the deformation processed Cr-Cu-Fe microcomposite wires combined with intermediate heat treatments have been investigated by [2001Son, 2002Kim]. The investigations were performed using samples of the Cu-1.2Cr-9Fe (mass%) composition. The primary and secondary dendrite arms were aligned along the deformation axis and elongated into filaments during cold drawing. It was shown that Cr atoms were mostly located in the Fe based filaments and the copper matrix was almost free of Cr atoms in agreement with the partition coefficient of Cr between the (Cu) and α or (Cu) and γ phases according to the alloy phase diagram. The filaments in Cr-Cu-Fe microcomposites were strengthened by the addition of Cr atoms and their refinement is relatively difficult due to the strengthening of filaments by Cr. Thermo-mechanical treatments have been employed by [2002Kim] to optimize the strength and conductivity of Cr-Cu-Fe microcomposites. The ultimate tensile strength and the conductivity of the Cu-1.2Cr-9Fe (mass%) wires drawn to the cold drawing strain $\eta = 4.8$ without intermediate heat treatments were observed to be 920 MPa and 33.8% IACS, respectively, and those with heat treatments were 891 MPa and 41% IACS. Further drawing wires to the cold drawing strain $\eta = 6.3$ after an additional heat treatment increased the conductivity from 43.1 to 53.3% IACS with a slight increase in hardness. The precipitation of impurities and alloying elements during intermediate heat treatments is thought to increase the conductivity due to reduced impurity scattering. Fig. 24 shows the variations of the strength and the ductility as a function of heat treatment temperature. The activation volumes for deformation increased from $138b^3$ in the as-drawn wire to $230b^3$ in the wire annealed at 500°C. Numerous particles were observed in Cu matrix, and the spacing between these particles was found to be slightly smaller than the activation length (138b = 35 nm). The most probable rate controlling mechanism of Cr-Cu-Fe microcomposites is suggested to be the interaction between dislocations and precipitates in Cu matrix.
The processes of sintering of Cr-Cu-Fe alloys with 2 to 18 mass% Cr and 2 and 4 mass% Cu using iron, copper and chromium or ferrochromium polvers as starting materials were studied by [1970Ahm,

1974Zap]. A notable homogenization degree of the alloys during the sintering process was reached at 1300°C after 12 h holding only. Examination of the diffusion phenomena and corrosion tests in nitric acid and magnesium chloride solution were carried out. While diffusion of Cr in Fe was found to slightly increase with Cu addition, microhardness and corrosion resistance increased with Cr addition markedly. The obtained diffusion coefficients of chromium in the α and γ phases as well as the corresponding activation energies are listed in Table 7.

The diffusion coefficients of copper and chromium in liquid Cr-Cu-Fe alloys at 1550°C were determined by [1975Wan], and the following values were obtained: $D_{Cu,Cu} = (5.5 \pm 0.1)\cdot10^{-5}$ cm^2·s^{-1}, $D_{Cu,Cr} = (-0.1 \pm 0.03)\cdot10^{-5}$ cm^2·s^{-1}, $D_{Cr,Cr} = (3.1 \pm 0.2)\cdot10^{-5}$ cm^2·s^{-1}, $D_{Cr,Cu} = (2.5 \pm 0.8)\cdot10^{-5}$ cm^2·s^{-1}.

Composite materials constituted of a Cu rich phase with a high electric conductivity and of a Fe rich phase with a high strength have an obvious advantage in terms of various properties. The preparation of such composite materials, however, is not easy by the powder metallurgical process because of diffusion problems, poor wetting between Cu and Fe [2001Les] and the high cost for fabrication. The formation of the core-type macroscopic morphology of as-cast Cr-Cu-Fe alloys due to the stable miscibility gap of the liquid phase is considered as useful peculiarity of the system for development of easy process of manufacture of the natural composites on the base of the conventional casting process [2004Wan].

Miscellaneous

The problem of hot shortness (cracking) of steels, induced by subscale enrichment of alloying elements during reheating before hot working, stimulated the investigation of the Cr effect on the Cu solubility in austenite and on the penetration of liquid copper rich phase down austenite grain boundaries. A slight decrease in the Cu solubility in austenite of mild steel when Cr content increased with a slight solubility minimum at 5 to 6 mass% Cr was found by [1967Sal] as mentioned above. Although the Cu solubility increased at higher Cr additions, but, with 9.38 mass% Cr, at 1250°C, it was still lower than that with no additions. Thus, the effect of Cr appears to be nearly neutral. However, because of a slight negative effect observed particularly over the critical temperature range at about 1100°C, Cr may be classified as a detrimental rather than beneficial addition.

The dihedral angle of the copper rich phase at the γ phase grain boundaries was measured by [1967Sal] to assess the effect of temperature on the penetration of the liquid copper rich phase into grain boundaries. The alloys containing more than 3 mass% chromium display a sharp decrease in the dihedral angle at about 1100°C. Minimum dihedral angle values, giving rise to maximum grain boundary penetration and probably maximum susceptibility of the steel to hot shortness are between 1075°C and 1175°C.

The multilayers Fe-X/Cu-8/Fe-Y/Cr/Fe-Y/Cu-8 show an inverse giant magnetoresistance [2001Mil]. The electrical conductivity of such multilayers decreases with the applied magnetic field. The electronic band contribution to the giant magnetoresistance for Fe-3/Cu-4/Fe/Cr/Fe/Cu-4 and Fe-3/Cu-4 multilayers was calculated within the semiclassical approximation. The results show a large change in the giant magnetoresistance behavior when one layer of Cr is introduced within the Fe layers. The dependence of impurity *vs* band effects in the appearance of inverse giant magnetoresistance in Cu/Fe superlattices with Cr was studied by [2002Mil]. The calculated giant magnetoresistance ratios have been compared with the experimental results, and it was concluded that the experimental data can only be explained by taking into account Cr bands.

Laser surface remelting/resolidifying treatment on a powder metallurgically manufactured Cr-Cu-Fe contact material was studied by [2000Gen]. A compact remelting/resolidifying layer was obtained with appropriate laser treatment conditions and a suitable surface absorption coating. After the treatment, the Cr-Cu-Fe microstructure of alloy on surface was greatly refined and the α phase was uniformly dispersed in the Cu rich matrix with a fine spherical or near spherical form. Improved compactness and microstructure of the laser remelted Cr-Cu-Fe material yielded increased hardness (up to 80%), wear resistance, and a reduced friction coefficient compared with the base material. The mechanism of laser strengthening was concerned with the microstructural features of the Cr-Cu-Fe material.

References

[1939Mor] Moriwaki, K., "The Equilibrium Diagram of the Ternary System, Iron-Chromium-Copper", *Tetsu to Hagane*, **25**, 396-403 (1939) (Phase Diagram, Experimental, 3)

[1967Sal] Salter, W.J.M., "Effect of Chromium on Solubility of Copper in Meld Steel", *J. Iron Steel Inst. Jpn.*, **205**, 1156-1160 (1967) (Phase Diagram, Experimental, 30)

[1970Ahm] Ahmed, M., Thuemmler, F., Zapf, G., "Metallographic Investigations of the Fe-Cr-Cu Alloys Prepared by Powder Metallurgical Methods", *Arch. Eisenhuettenwes.*, **41**, 797-803 (1970) (Phase Diagram, Mechan. Prop., Experimental, 25)

[1971Yam] Yamaguchi, M., Ymakoshi, Y., Mima G., "Miscibility Gap in the Iron-Chromium-Metal (X=Copper, Manganese, Molybdenum, Nickel, Vanadium, Silicon and Aluminium) System", *Proc. Int. Conf. Sci. Technol. Iron Steel*, Tokyo, **2**, 1015-1019 (1971) (Phase Relations, Experimental, 35)

[1974Sig] Sigworth, G.K., Elliott, J.F., "The Thermodynamics of Liquid Dilute Iron Alloys", *Met. Sci.*, **8**, 298-310 (1974) (Thermodyn., Review, 249)

[1974Zap] Zapf, G., Ahmed, M., "Research Report of the State of Noth Rhine-Westphalia, No. 2430: Investigations on the Sinter Alloying of the Binary Iron-Chromium System and the Ternary Iron-Chromium-Copper System (Forschungsbericht Des Landes Nordrheim)", Westdeutscher Verlag, Opladen, Germany, 149 pp (1974) (Phase Diagram, Mechan. Properties, Experimental, 88)

[1975Wan] Wanibe, Y., Takagi, T., Sakao, H., "Coupling Phenomenon in the Ternary Isothermal Diffusion of Liquid Iron-Chromium-Copper Alloys", *Arch. Eisenhuettenwes.*, **46**(9), 561-565 (1975) (Transport Phenomena, Experimental, 7)

[1979Cha] Chang, Y.A., Neumann, J.P., Mikula, A., Goldberg, D., "Cr-Cu-Fe", *INCRA Monograph Series 6. Phase Diagrams and Thermodynamic Properties of Ternary Copper-Metall Systems*, NSRD, Washington, 439-446 (1979) (Phase Diagram, Review, 6)

[1987And] Anderson, J.O., Sundman, B., "Thermodynamic Properties of the Cr-Fe System", *Calphad*, **11**, 83-92 (1987) (Calculation, Phase Diagram, Thermodyn., Assessment) as cited in [2002Wan]

[1988Uen] Ueno, S., Waseda, Y., Jacob, K.T., Tamaki, S., "Theoretical Treatment of Interaction Parameters in Multicomponent Metallic Solutions", *Steel Res.*, **59**(11), 474-483 (1988) (Thermodyn., Theory, Calculation, 44)

[1990Ham] Haemaelainen, M., Jaaskelainen, K., Luoma, R., Nuotio, M., Taskinen, P., Teppo, O.A., "Thermodynamic Analysis of the Binary Alloy Systems Cu-Cr, Cu-Nb and Cu-V", *Calphad*, **14**(2), 125-137 (1990) (Calculation, Phase Diagram, Thermodyn., Assessment, 52)

[1993Hao] Hao, S.M., Jiang, M., "Cr-Cu-Fe", *Proc. 7th Nat. Symp. Phase Diagrams, Chinese Phys. Soc.,* Shanghai, 11-13 (1993) (Phase Diagram, Experimental, 0)

[1995Che] Chen, Q., Jin, Z., "The Fe-Cu System: a Thermodynamic Evaluation", *Metal. Mater. Trans. A*, **26A**(2), 417-426 (1995) (Calculation, Phase Diagram, Thermodyn., Assessment, 55)

[1997Oht] Ohtani, H., Suda, H., Ishida, K., "Solid/Liquid Equilibria in Fe-Cu Based Ternary Systems", *ISIJ Int.*, **37**(3), 207-216 (1997) (Experimental, Calculation, Phase Relations, Review, Thermodyn., 47)

[1998Mie] Miettinen, J., "Approximate Thermodynamic Solution Phase Data for Steels", *Calphad*, **22**(2), 275-300 (1998) (Review, Calculation, 83)

[2000Gen] Geng, H.R., Liu, Y., Chen, C.Z., Sun, M.H., Gao, Y.Q., "Laser Surface Remelting of Cu-Cr-Fe Contact Material", *Mater. Sci. Technol.*, **16**(5), 564-567 (2000) (Experimental, Morphology, Mechan. Prop., Electr. Prop.) cited from abstract

[2001Fer1] Fernee, H., Nairn, J., Atrens, A., "Cu-Rich Corner of the Cu-Fe-Cr Phase Diagram", *J. Mater. Sci. Lett.*, **20**, 2213-2215 (2001) (Experimental, Electr. Prop., Phase Relations, 6)

[2001Fer2] Fernee, H., Nairn, J., Atrens, A., "Cold Worked Cu-Fe-Cr Alloys", *J. Mater. Sci.*, **36**(22), 5497-5510 (2001) (Electr. Prop., Mechan. Prop., Experimental, 19)

[2001Fer3] Fernee, H., Nairn, J., Atrens, A., "Precepitation Hardening of Cu-Fe-Cr Alloys - Part 1 - Mechanical and Electrical Properties", *J. Mater. Sci.*, **36**(11), 2711-2719 (2001) (Experimental, Electr. Prop., Mechan. Prop., 19)

[2001Les] Lesnik, N.D., Minakova, R.V., Khomenko, E.V., "Chromium-Copper System: Adhesion Characteristics, Doping, the Structure of Phase Boundary and Composites", *Powder Metall. Met. Ceram.*, **40**(7-8), 432-440 (2001) (Experimental, Morphology, Phys. Prop., Interface Phenomena, 12)

[2001Mil] Milano, J. Llois, A.M., "From Direct to Inverse GMR: Introduction of Cr in Fe/Cu Superlattices", *J. Mag. Mag. Mater.*, **226**, 1755-1757 (2001) (Calculation, Magn. Prop.) cited from abstract

[2001Son] Song, J.S., Hong, S.I., Kim, H.S., "Heavily Drawn Cu-Fe-Ag and Cu-Fe-Cr Microcomposites", *J. Mat. Proc. Tech.*, **113**(1-3), 610-616 (2001) (Experimental, Mechan. Prop., Morphology, 21)

[2002Ans] Ansara, I., Ivanchenko, V., "Cr - Cu (Chromium - Copper)", MSIT Binary Evaluation Program, in *MSIT Workplace*, Effenberg, G. (Ed.), MSI, Materials Science International Services GmbH, Stuttgart; Document ID: 20.19588.1.20, (2002) (Crys. Structure, Phase Diagram, Assessment, 29)

[2002Kim] Kim, Y.S., Song, J.S., Hong, S.I., "Thermo-Mechanical Properties of Cu-Fe-Cr Microcomposites", *J. Mat. Proc. Tech.*, **130**, 278-282 (2002) (Experimental, Mechan. Prop., Morphology, 23)

[2002Mil] Milano, J., Llois, A.M., Steren, L.B., "Combined Impurity and Band Effects on the Appearance of Inverse Giant Magnetoresistance in Cu/Fe Multilayers with Cr", *Phys. Rev. B*, **66**(13), Art. No. 134405 (2002) (Calculation, Magn. Prop.) cited from abstract

[2002Rag] Raghavan, V., "Cr-Cu-Fe (Chromium-Copper-Iron)", *J. Phase Equilib.*, **23**(3), 257-258 (2002) (Review, Phase Relations, 5)

[2002Wan] Wang, C.P., Liu, X.J., Ohnuma, I., Kainuma, R., Ishida, K., "Phase Equilibria in Fe-Cu-X (X: Co, Cr, Si, V) Ternary Systems", *J. Phase Equilib.*, **23**(3), 236-245 (2002) (Experimental, Calculation, Phase Diagram, Thermodyn., #, 38)

[2004Wan] Wang, C.P., Liu, X.J., Takaku, Y., Ohnuma, I., Kainuma, R., Ishida, K., "Formation of Core-Type Macroscopic Morphologies in Cu-Fe Base Alloys with Liquid Miscibility Gap", *Metall. Mater. Trans. A*, **35A**(4), 1243-1253 (2004) (Experimental, Calculation, Morphology, Phase Diagram, Thermodyn., 31)

[2006Tur] Turchanin, M., Agraval P., "Cu - Fe (Copper - Iron)", MSIT Binary Evaluation Program, in *MSIT Workplace*, Effenberg, G. (Ed.), MSI, Materials Science International Services GmbH, Stuttgart; to be published (2006) (Crys. Structure, Phase Diagram, Thermodyn., Assessment, 36)

Table 1: Investigations of the Cr-Cu-Fe Phase Relations and Structures

Reference	Method/Experimental Technique	Temperature/Composition/Phase Range Studied
[1939Mor]	DTA, dilatometric measurements, optical microscopy	Temperature-composition sections: at 2 mass% Cr and 0 to 20 mass% Cu; at 5 mass% Cr and 0 to 40 mass% Cu; at 14 mass% Cr and 0 to 40 mass% Cu; at 1 mass% Cu and 4 to 20 mass% Cr; at 2 mass% Cu and 4 to 20 mass% Cr; at 4 mass% Cu and 4 to 20 mass% Cr; at 6 mass% Cu and 4 to 20 mass% Cr
[1967Sal]	Optical microscopy, EPMA, Cr-Cu-mild steel alloys	Partial isothermal sections: at 900°C ((Cu)/γ phase boundaries); at 1100 and 1250°C ((L)/γ phase boundaries)
[1970Ahm, 1974Zap]	Optical microscopy, dilatometric measurements, DTA, X-ray analysis	Temperature-composition sections: at 2 mass% Cu and 2 to 18 mass% Cr; at 4 mass% Cu and 2 to 18 mass% Cr α/γ phase boundaries
[1971Yam]	Optical microscopy, DTA	Influence of Cu additions on the miscibility gap in the α-phase
[1993Hao]	Diffusion couples technique, optical microscopy, EPMA	Isothermal section at 1000°C, (Cu)/γ, (Cu)/ α and α/γ phase boundaries
[1997Oht]	Solid-liquid diffusion couples technique, SEM-Electron Dispersive X-ray analysis	Partial isothermal sections at 1100, 1200, 1300°C, (L)/γ and (L)/α phase boundaries
[2001Fer1]	Wavelength dispersive spectroscopy, resistivity measurements	Partial isothermal section at 1050°C, (Cu)-phase
[2002Wan]	SEM-Electron Dispersive X-ray analysis	Partial isothermal sections: at 800°C, (Cu)/α phase boundaries; at 900°C, (Cu)/γ phase boundaries; at 1000°C, (Cu)/γ phase boundaries; at 1200°C, (L)/γ phase boundaries
[2004Wan]	Optical microscopy	49 to 65 mass% Cu, 34 to 49.5 mass% Fe, 2 to 7.2 mass% Cr, miscibility gap in liquid phase

Table 2: Crystallographic Data of Solid Phases

Phase/ Temperature Range [°C]	Pearson Symbol/ Space Group/ Prototype	Lattice Parameters [pm]	Comments/References
(Cu), $Cr_xCu_yFe_{1-x-y}$ < 1084.62	*cF*4 *Fm*$\bar{3}$*m* Cu		at $x = 0$ and 1096°C, $0.955 \le y \le 1$ [1995Che]
			at $x + y = 1$ and 1075°C, $0.9992 \le y \le 1$ [1990Ham]
		$a = 361.46$	at $x = 0$, $y = 1$ and 25°C [V-C2, Mas2]
γ, $Cr_xCu_yFe_{1-x-y}$ 1486 - 849	*cF*4 *Fm*$\bar{3}$*m* Cu		at $x = 0$, $0 \le y \le 0.13$ [1995Che]
			at $y = 0$ and 977°C, $0 \le x \le 0.12$ [1987And]
(γFe) 1394 - 912		$a = 364.68$	at $x = 0$, $y = 0$ and 912°C [V-C2, Mas2]
α, $Cr_xCu_yFe_{1-x-y}$ < 1863	*cI*2 *Im*$\bar{3}$*m* W		at $x = 0$ and 1486°C, $0 \le y \le 0.063$
			at $x = 0$ and 849°C, $0 \le y \le 0.017$ [1995Che]
			at $y = 0$, $0 \le x \le 1$ [1987And]
			at $x + y = 1$ and 1557°C, $0 \le y \le 0.0034$ [1990Ham]
(Cr) < 1863		$a = 288.48$	at $x = 1$, $y = 0$ and 25°C [V-C2, Mas2]
(δFe) 1538 - 1394		$a = 293.15$	at $x = 0$, $y = 0$ and 1394°C [V-C2, Mas2]
(αFe) < 912		$a = 293.22$	at $x = 0$, $y = 0$ and 25°C [V-C2, Mas2]
σ, Cr_xFe_{1-x} 831 - 510	*tP*30 $P4_2/mnm$ CrFe		at 831°C, $x = 0.45$
			at 510°C, $x = 0.51$
			at 700°C, $0.44 \le x \le 0.5$ [1987And]
		$a = 879.66$ $c = 455.82$	at 650 - 790°C and $x = 0.495$ [V-C2]

Table 3: Invariant Equilibria

Reaction	*T* [°C]	Type	Phase	Composition (at.%)		
				Cu	Cr	Fe
L, L', L"	1523	c_1(critical)	L	48.0	33.0	19.0
L', L", α	1516	c_2(critical)	L', L"	48.8	41.5	9.7
			α	1.0	84.4	14.6
L', L", γ	1431	c_3(critical)	L', L"	53.4	1.7	44.9
			γ	14.0	2.1	83.9
L' + γ ⇌ L" + α	1396	U_1	L'	25.1	9.7	65.2
			γ	11.1	8.6	80.3
			L"	77.0	2.9	20.1
			α	8.6	10.2	81.2

Reaction	T [°C]	Type	Phase	Composition (at.%)		
				Cu	Cr	Fe
L' ⇌ L" + α	1362	e_1(min)	L'	18.8	25.7	55.5
			L"	84.2	5.7	10.1
			α	6.3	29.7	64.0
L + γ ⇌ α + (Cu)	1088	U_2	L	96.7	0.7	2.6
			γ	5.7	14.7	79.6
			α	3.9	18.3	77.8
			(Cu)	96.3	0.3	3.4

Table 4: Equilibrium Compositions of the α, γ and Liquid Phases in the Three-Phase Region

T [°C]	Phase	Composition (at.%)		
		Cu	Cr	Fe
1300	L	89.7	1.8	8.5
	α	7.1	13.4	79.5
	γ	9.5	11.3	79.3
1250	L	92.2	1.6	6.2
	α	6.3	14.9	78.8
	γ	8.5	12.3	79.2
1200	L	94.1	1.2	4.7
	α	5.5	16.1	78.4
	γ	7.6	13.2	79.2
1100	L	96.5	0.8	2.7
	α	4.0	18.2	77.8
	γ	5.9	14.5	79.6

Table 5: Equilibrium Compositions of the α, γ and (Cu) Phases in the Three-Phase Region

T [°C]	Phase	Composition (at.%)		
		Cu	Cr	Fe
1050	(Cu)	96.9	0.2	2.9
	α	3.3	18.6	78.1
	γ	4.9	14.8	80.3
1000	(Cu)	97.5	0.2	2.3
	α	2.6	18.8	78.6
	γ	3.9	15.0	81.1
900	(Cu)	98.5	0.1	1.4
	α	1.6	17.8	80.6
	γ	2.5	14.4	83.1
850	(Cu)	98.8	0.1	1.1
	α	1.2	15.8	83.0
	γ	2.0	13.3	84.7

Table 6: Investigations of the Cr-Cu-Fe Materials Properties

Reference	Method/Experimental Technique	Type of Property
[1967Sal]	Optical microscopy	Dihedral angle measurements at 1 to 15 mass% Cu, 0 to 9.38 mass% Cr and at 900 to 1250°C
[1970Ahm, 1974Zap]	Diffusion couple method	Homogenization degree of sintered of Cr-Cu-Fe alloys with 2 to 18 mass% Cr and 2 to 4 mass% Cu at 1050 to 1410°C, diffusion coefficient and activation energy of diffusion of Cr in α and γ phases.
	Corrosion tests, micro-hardness tests	Microhardness and corrosion resistance
[1975Wan]	Diffusion couple method	Diffusion coefficients of copper and chromium in liquid Cr-Cu-Fe alloys at 1550°C
[2000Gen]	Optical microscopy, friction tests, resistance tests, hardness tests	Mechanical and electrical properties of laser surface remelting/resolidifying processed Cr-Cu-Fe contact material manufactured by powder metallurgy
[2001Fer1]	Resistivity measurements	Temperature dependence of resistivity of Cu rich alloys at < 1 mass% Fe, < 0.6 mass% Cr and at 500 to 1050°C
[2001Fer2]	Electrical conductivity measurements, optical microscopy, TEM, WDS, hardness tests	Microstructure, electrical and mechanical properties of Cu - 0.7 mass% Cr - 0.3 mass% Fe, Cu - 0.7 mass% Cr - 0.8 mass% Fe and Cu - 0.7 mass% Cr - 2.0 mass% Fe alloys
[2001Fer3]	TEM, WDS, hardness tests, resistivity measurements	Microstructure, electrical and mechanical properties of Cu - 0.7 mass% Cr - 2.0 mass% Fe cold-worked alloy
[2001Les]	Stationary-drop method tests of wettability, optical microscopy, electron microscopy, EPMA	Adhesive characteristics and formation of phase boundaries in Cu rich composite materials manufactured by powder metallurgical process at 1100-1300°C
[2001Son]	Mechanical properties tests using extensometer, optical microscopy, SEM, resistivity tests using four-probe technique	Microstructure, mechanical and electrical properties of deformation processed Cu - 1.2 mass% Cr - 9 mass% Fe microcomposite wires
[2002Kim]	Mechanical strength tests using machine equipped with extensometer, Vickers micro-hardness tests, image analysis, TEM	Ultimate tensile strength and the conductivity of deformation processed Cu - 1.2 mass% Cr - 9 mass% Fe microcomposite wires
[2004Wan]	Optical microscopy	Core type macroscopic morphologies

Table 7: Diffusion Coefficient and Activation Energy of Diffusion of Cr in α and γ Phases

Diffusion Couple	Diffusion Coefficient [$cm^2 \cdot s^{-1}$] at Sintering Temperature					Q_α [$kJ \cdot g\text{-}atom^{-1}$]	Q_γ [$kJ \cdot g\text{-}atom^{-1}$]
	1410°C	1250°C		1050°C			
	D_α	D_α	D_γ	D_α	D_γ		
(Fe-Cr)/Fe	$1.7 \cdot 10^{-7}$	$3.2 \cdot 10^{-8}$	$4.6 \cdot 10^{-10}$	$1.9 \cdot 10^{-9}$	$4.2 \cdot 10^{-11}$	239.3248	212.1288
(Fe-Cr + 2%Cu)/Fe	$2.2 \cdot 10^{-7}$	$2.8 \cdot 10^{-8}$	$1.7 \cdot 10^{-9}$	$8.2 \cdot 10^{-10}$	$1.7 \cdot 10^{-10}$	298.7376	194.9744
(Fe-Cr)/(Fe + 2%Cu)	$1.2 \cdot 10^{-7}$	$1.3 \cdot 10^{-8}$	$4.2 \cdot 10^{-10}$	$3.0 \cdot 10^{-10}$	$3.0 \cdot 10^{-11}$	308.7792	233.0488
(Fe-Cr + 2%Cu)/(Fe + 2%Cu)	$1.5 \cdot 10^{-7}$	$2.8 \cdot 10^{-8}$	$5.0 \cdot 10^{-10}$	$1.4 \cdot 10^{-9}$	$6.5 \cdot 10^{-11}$	251.8768	176.9832
(Fe-Cr + 4%Cu)/Fe	$2.2 \cdot 10^{-7}$	$4.2 \cdot 10^{-8}$	$3.6 \cdot 10^{-9}$	$3.0 \cdot 10^{-9}$	$3.9 \cdot 10^{-10}$	227.6096	195.3928
(Fe-Cr)/(Fe + 4%Cu)	$1.5 \cdot 10^{-7}$	$2.7 \cdot 10^{-8}$	$8.5 \cdot 10^{-10}$	$1.4 \cdot 10^{-9}$	$9.4 \cdot 10^{-11}$	256.0608	187.4432
(Fe–Cr + 4%Cu)/(Fe + 4%Cu)	$1.5 \cdot 10^{-7}$	$1.6 \cdot 10^{-8}$	$8.0 \cdot 10^{-10}$	$3.1 \cdot 10^{-10}$	$6.5 \cdot 10^{-11}$	329.6992	216.7312
(Fe–Cr)/Cu/Fe	-	$1.5 \cdot 10^{-8}$	$3.8 \cdot 10^{-9}$	-	-	239.3248	212.1288

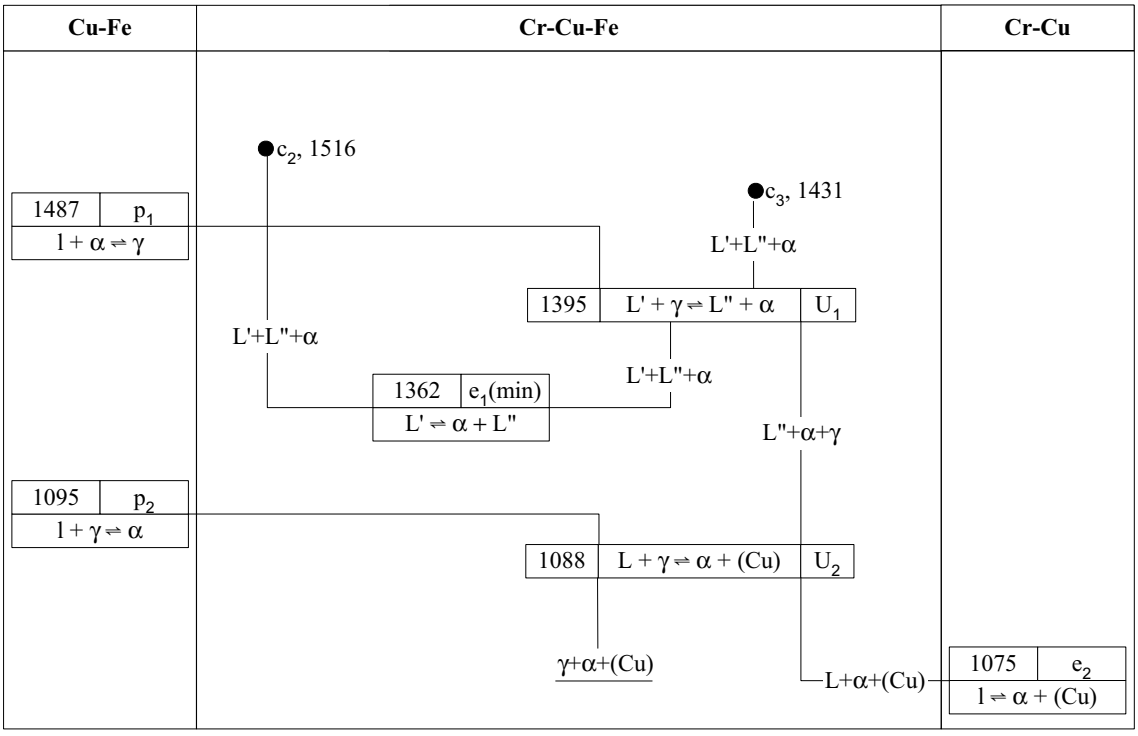

Fig. 1: Cr-Cu-Fe. Reaction scheme

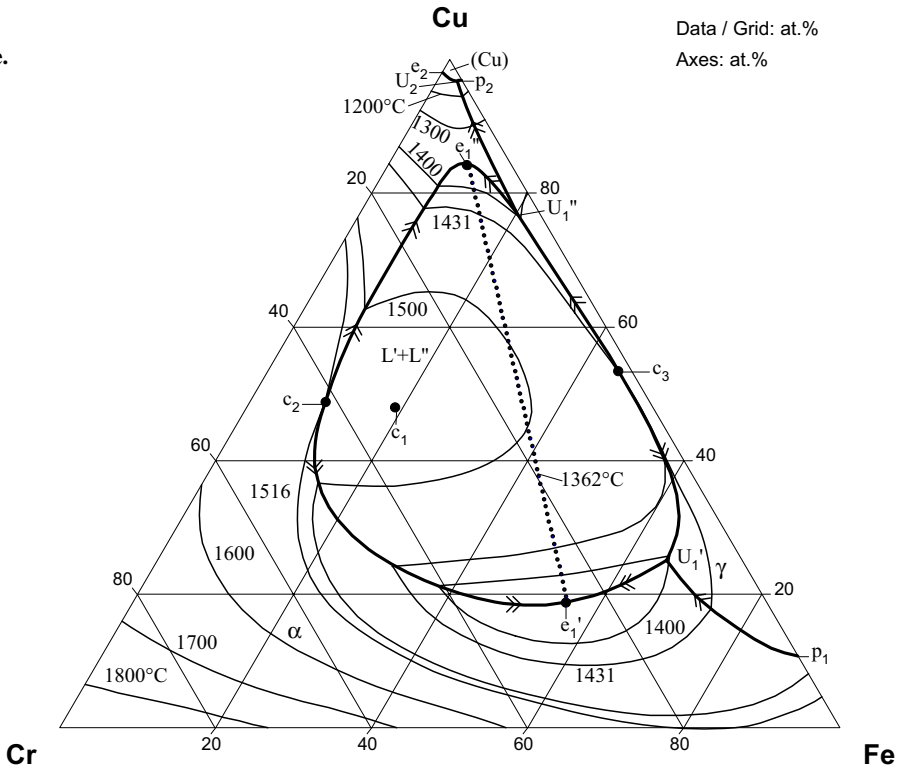

Fig. 2a: Cr-Cu-Fe. Calculated liquidus projection

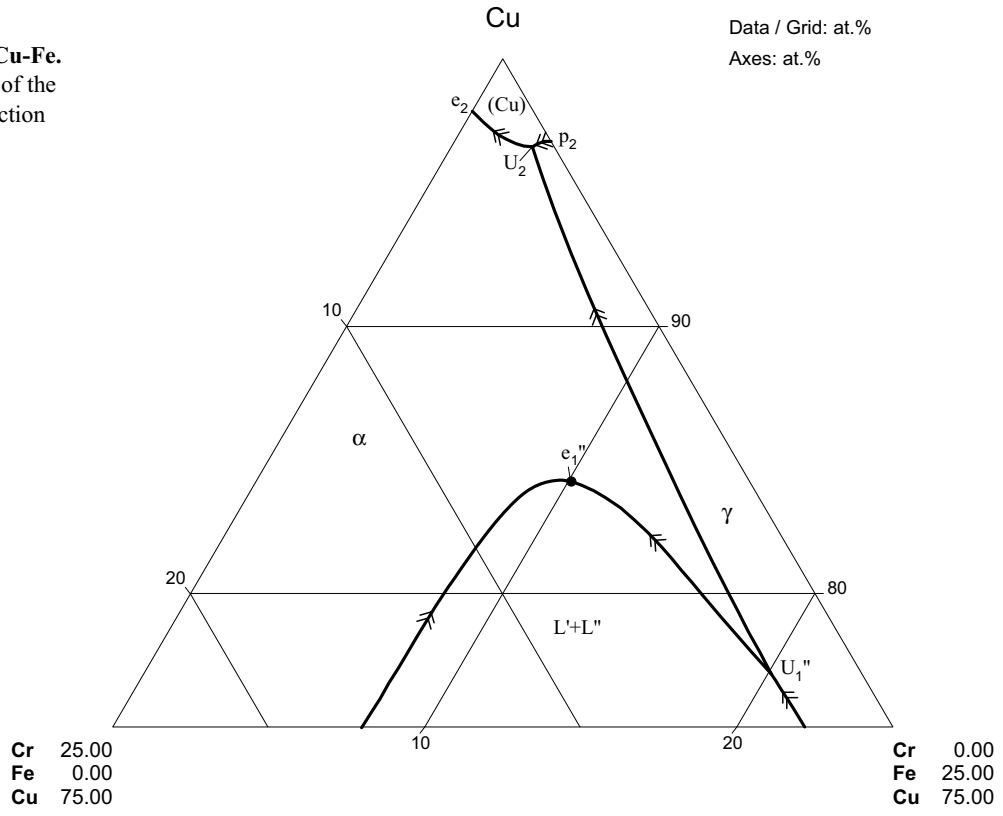

Fig. 2b: Cr-Cu-Fe. Enlarged part of the liquidus projection

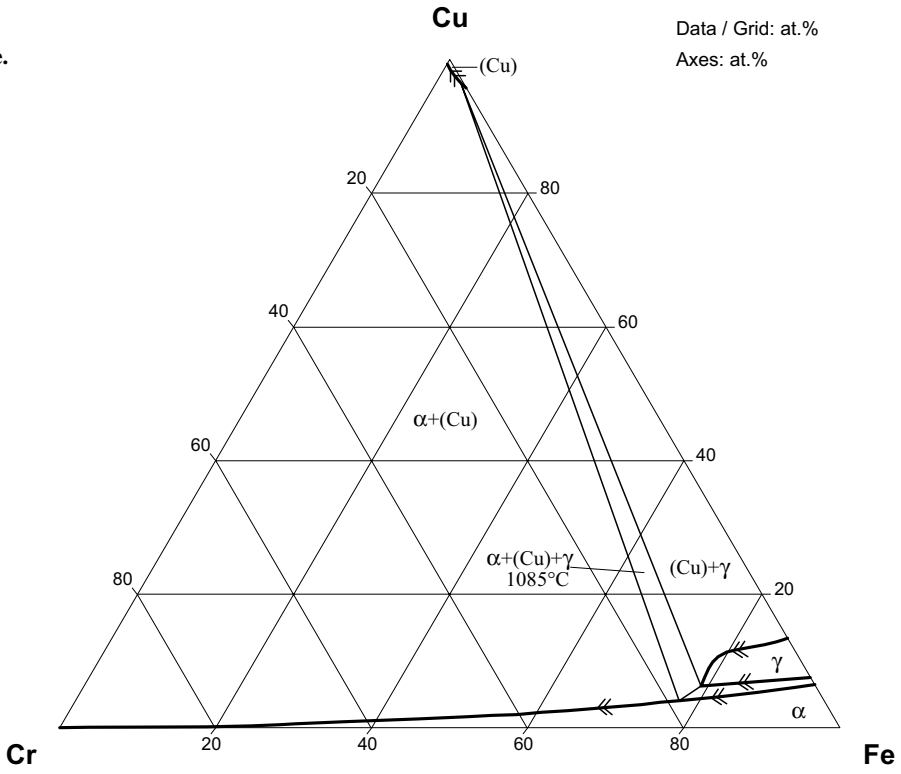

Fig. 3: Cr-Cu-Fe. Solidus surface projection

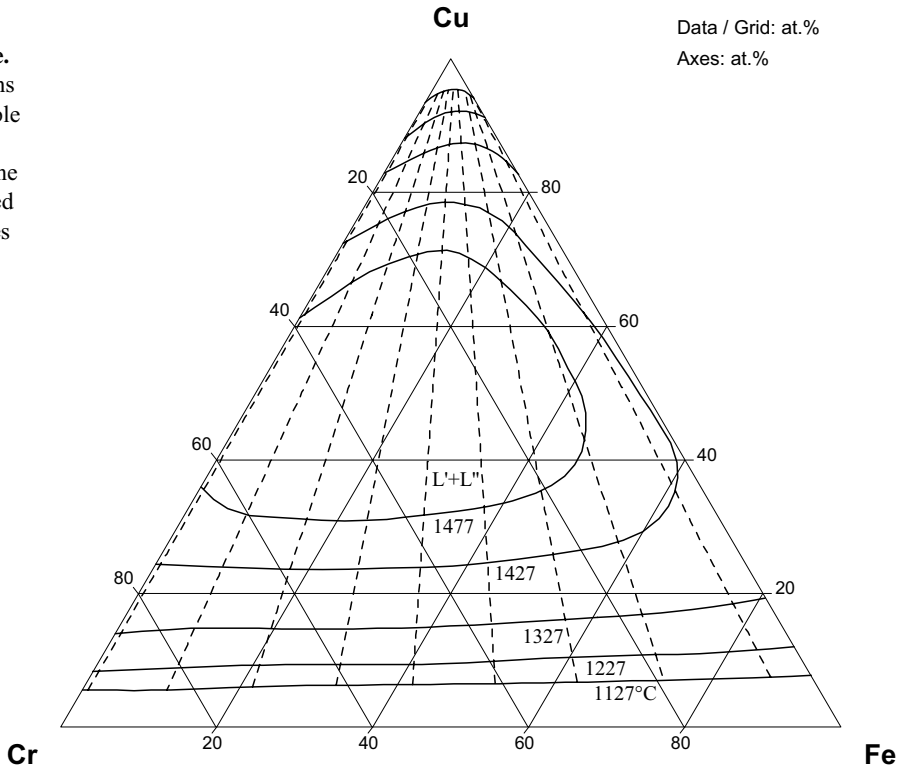

Fig. 4: Cr-Cu-Fe. Calculated isotherms of the cupola of stable and metastable miscibility gap of the liquid phase. Dashed lines are the tie lines at 1127°C.

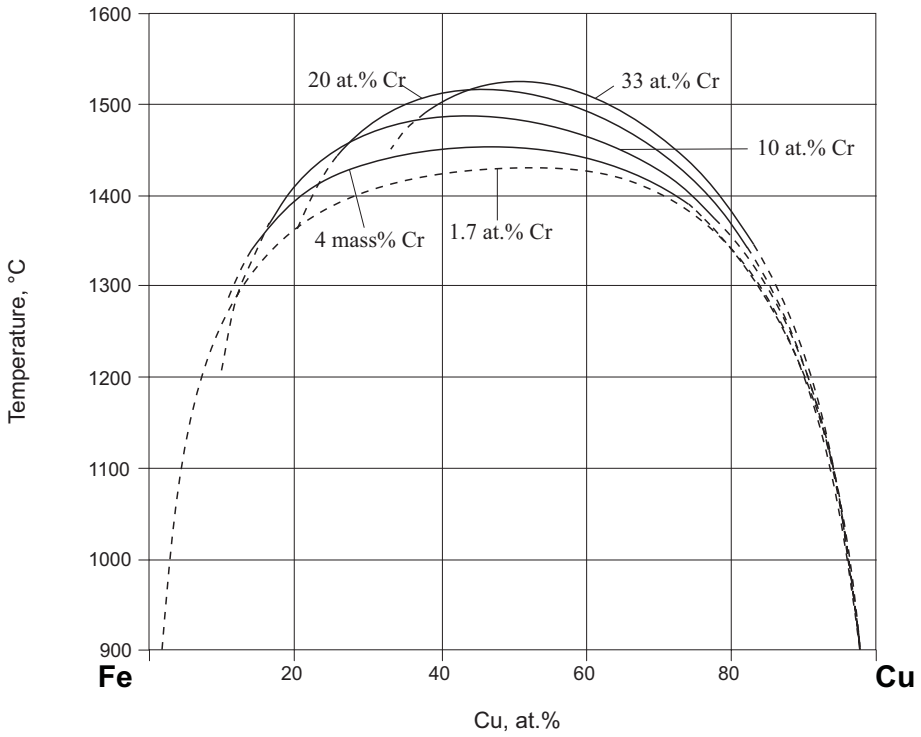

Fig. 5: Cr-Cu-Fe. Calculated vertical sections of the miscibility gap. Solid lines correspond to the stable range and dashed lines correspond to the metastable range, section at 4 mass% Cr is taken from [2004Wan]

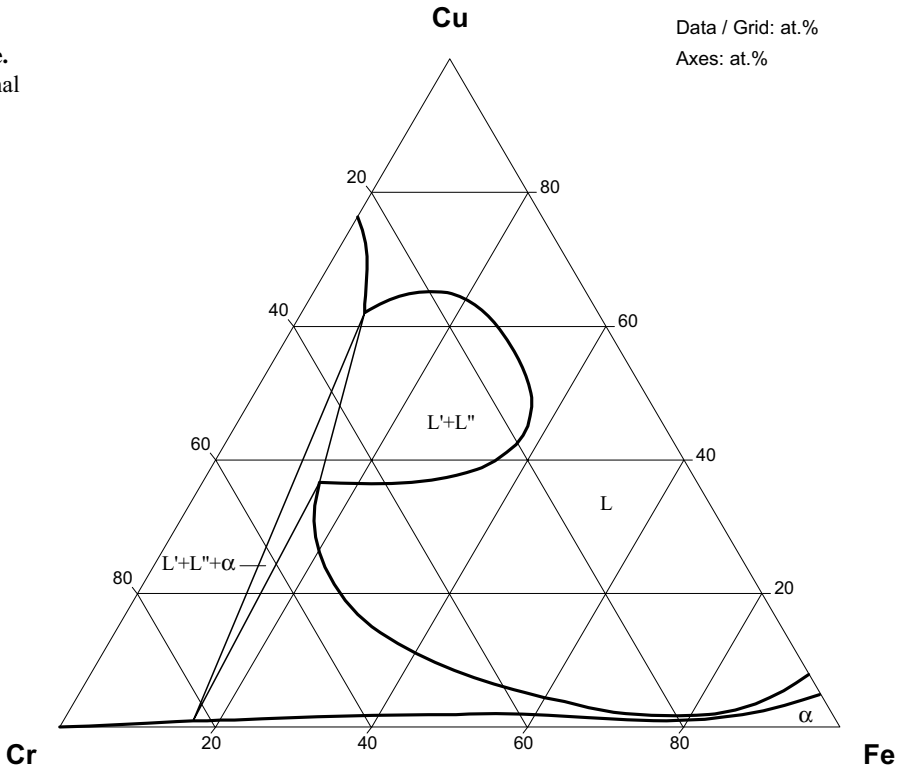

Fig. 6: Cr-Cu-Fe. Calculated isothermal section at 1500°C

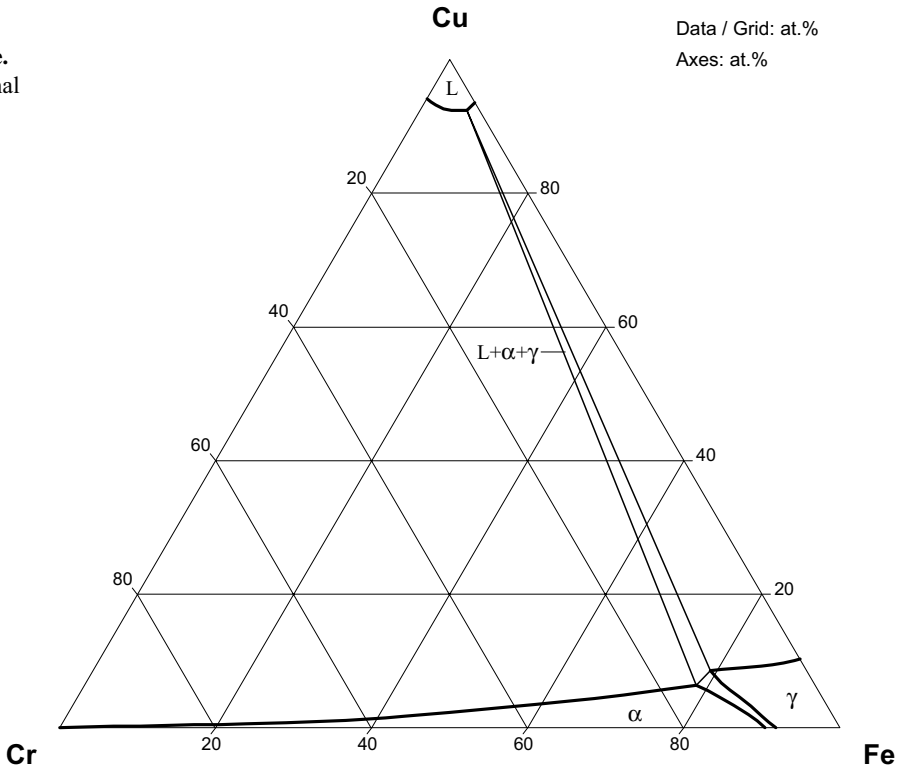

Fig. 7: Cr-Cu-Fe. Calculated isothermal section at 1250°C

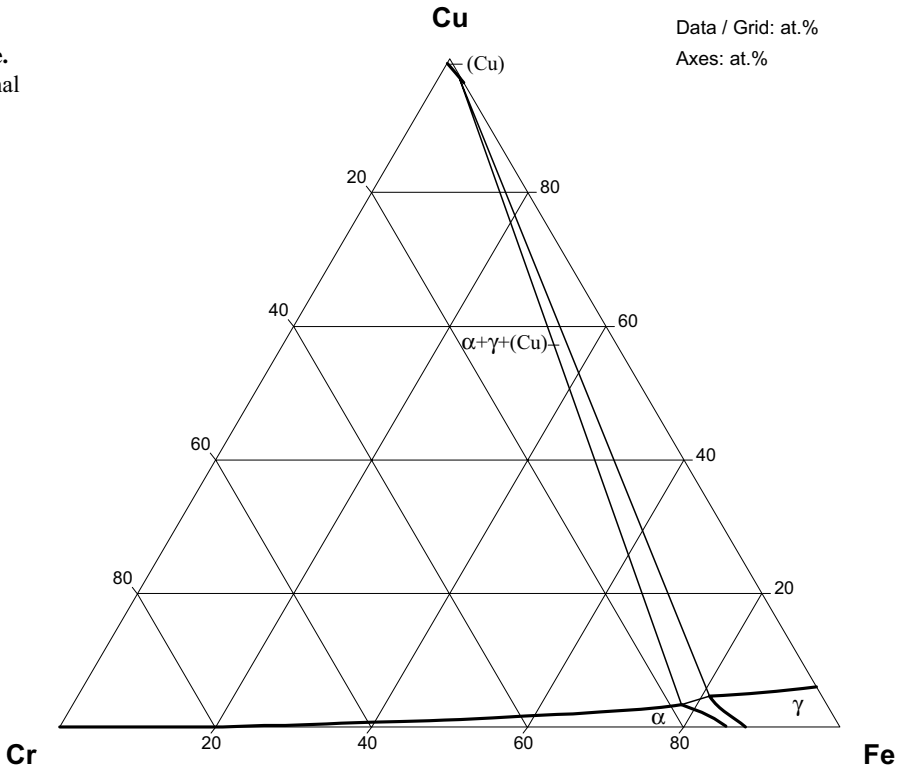

Fig. 8: Cr-Cu-Fe. Calculated isothermal section at 1050°C

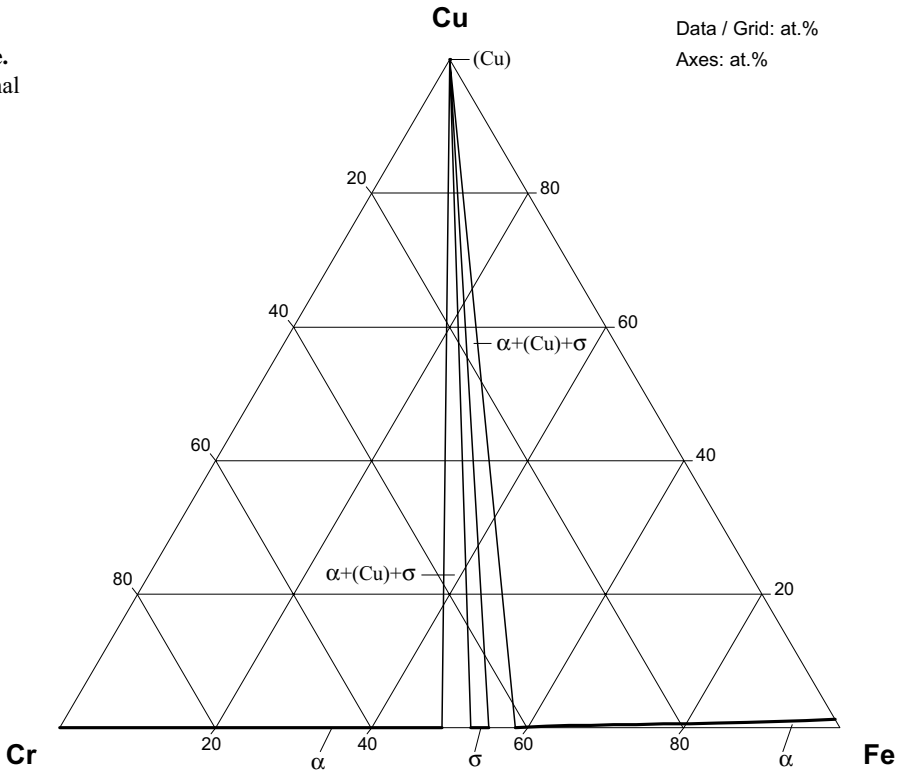

Fig. 9: Cr-Cu-Fe. Calculated isothermal section at 800°C

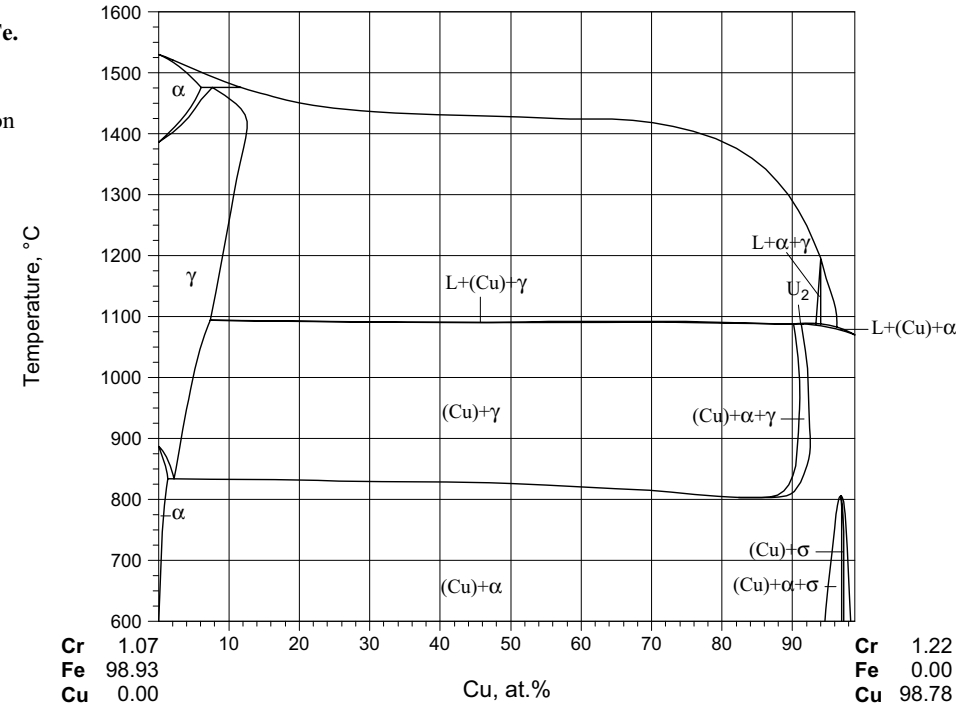

Fig. 10: Cr-Cu-Fe. Calculated temperature-composition section at 1 mass% Cr, plotted in at.%

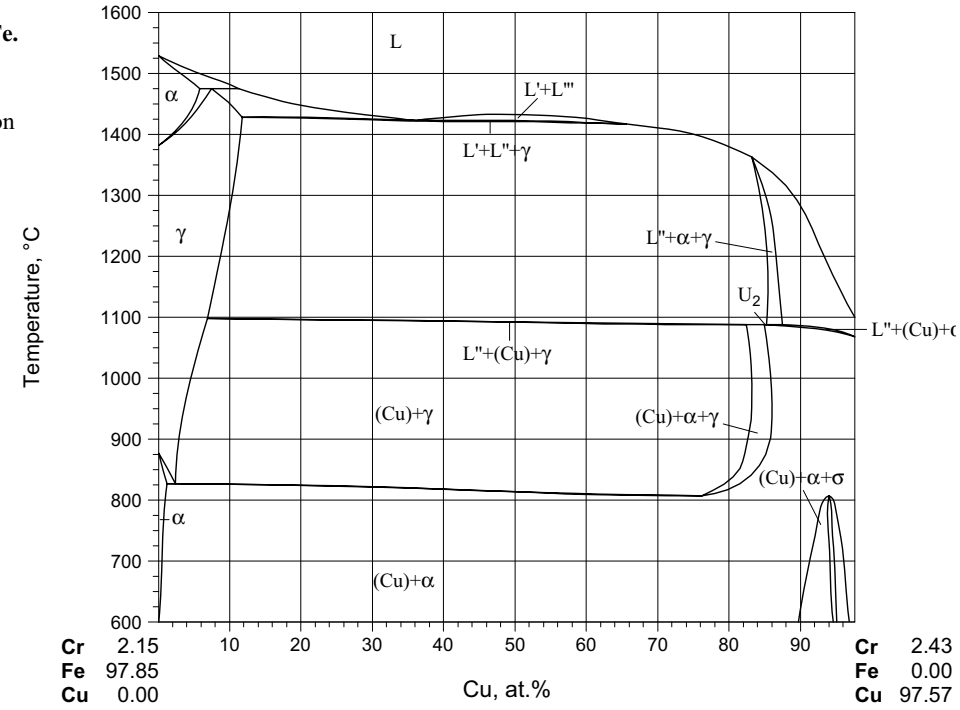

Fig. 11: Cr-Cu-Fe. Calculated temperature-composition section at 2 mass% Cr, plotted in at.%

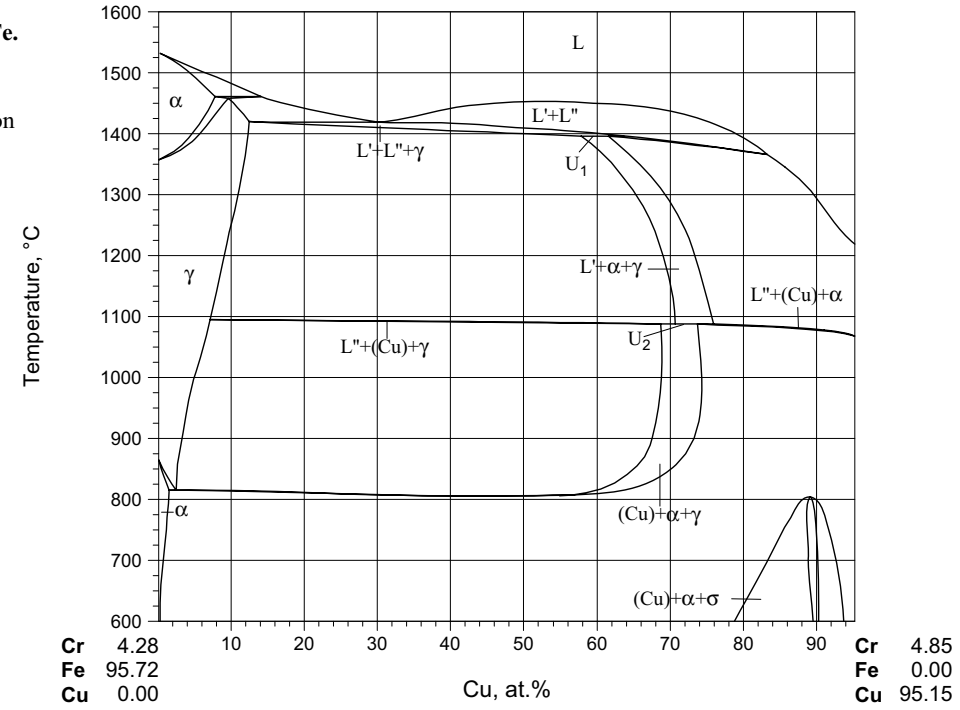

Fig. 12: Cr-Cu-Fe. Calculated temperature-composition section at 4 mass% Cr, plotted in at.%

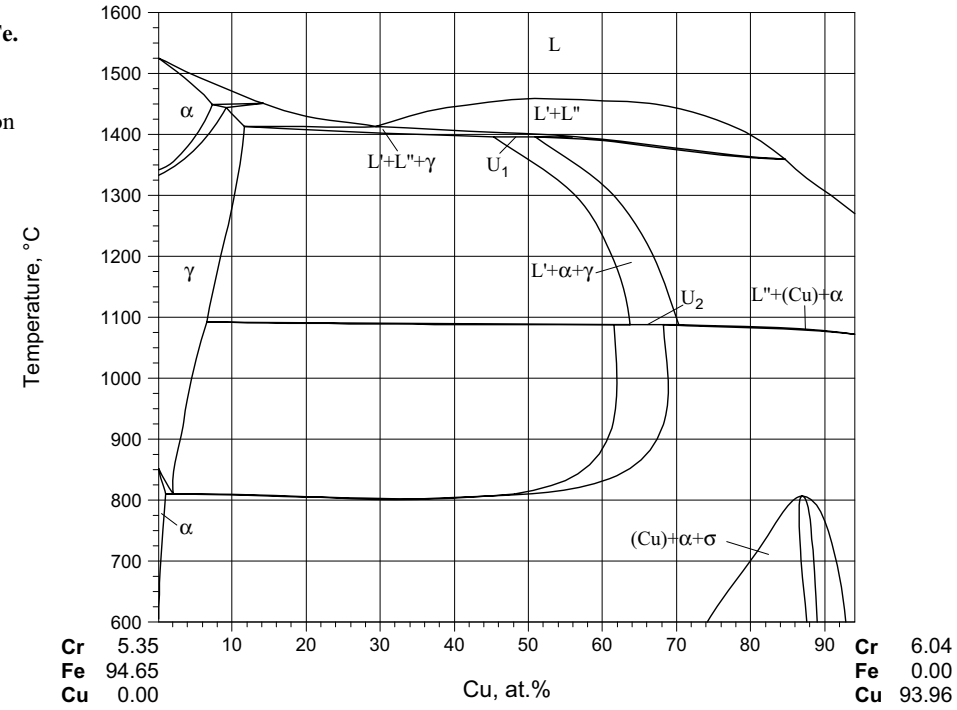

Fig. 13: Cr-Cu-Fe. Calculated temperature-composition section at 5 mass% Cr, plotted in at.%

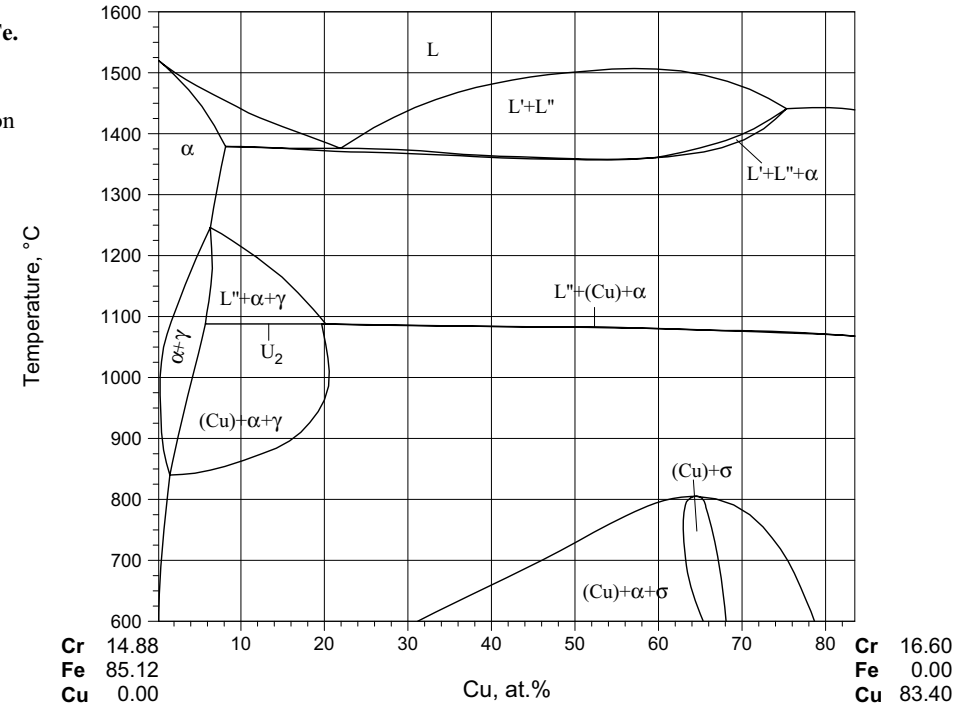

Fig. 14: Cr-Cu-Fe. Calculated temperature-composition section at 14 mass% Cr, plotted in at.%

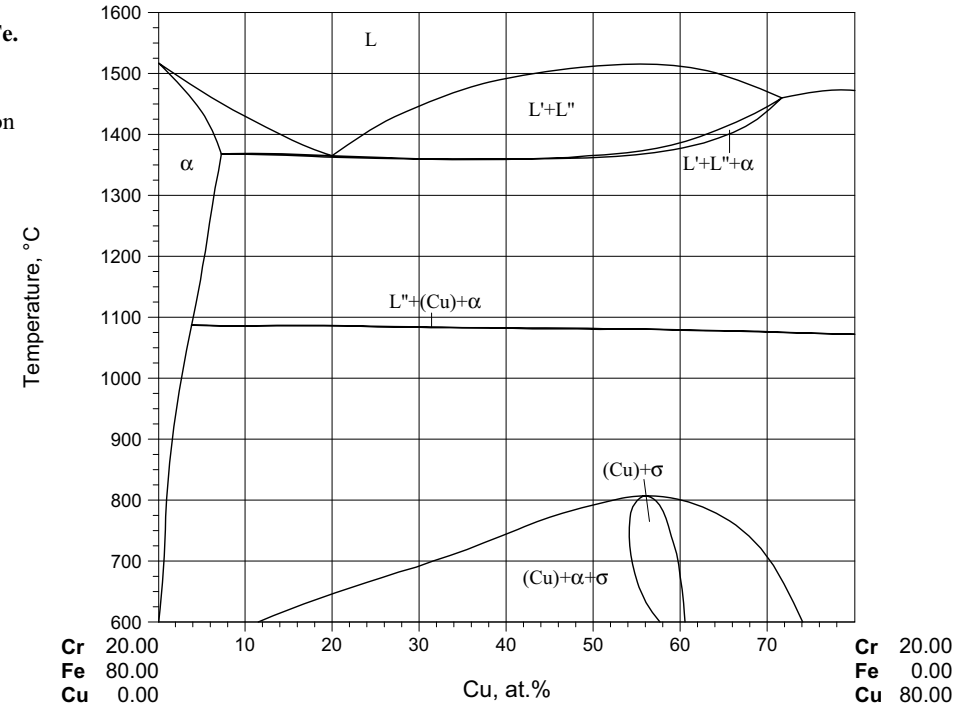

Fig. 15: Cr-Cu-Fe. Calculated temperature-composition section at 20 at.% Cr

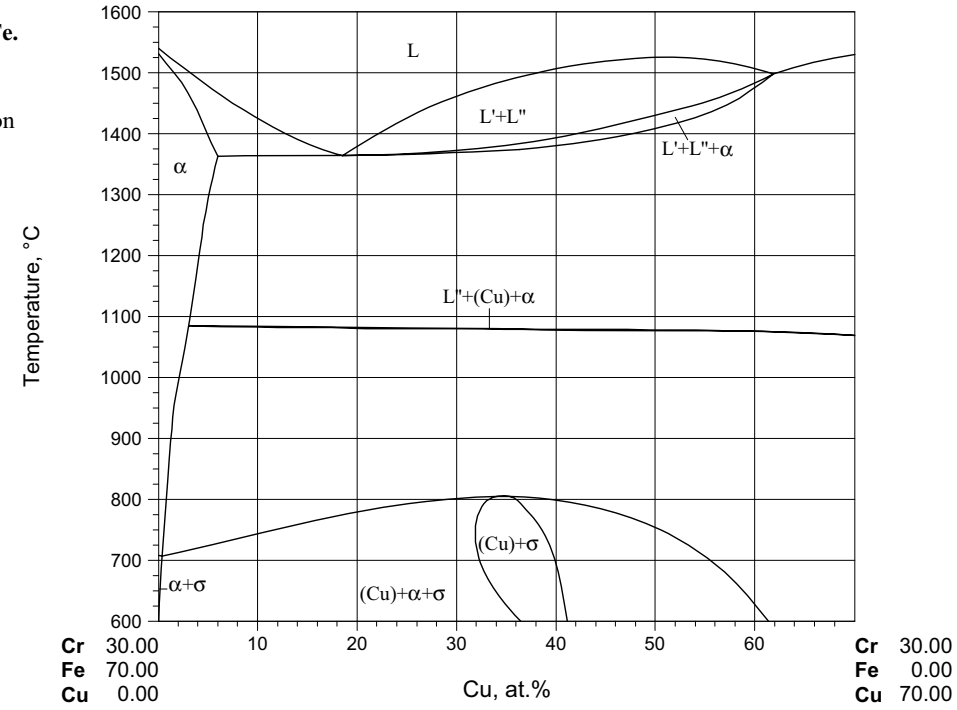

Fig. 16: Cr-Cu-Fe. Calculated temperature-composition section at 30 at.% Cr

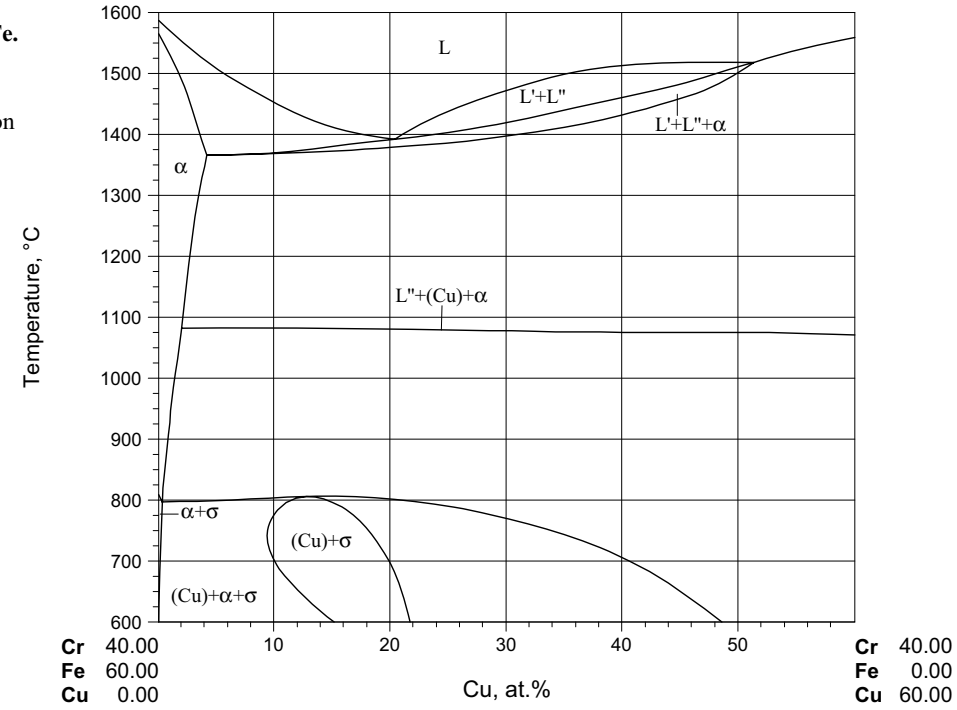

Fig. 17: Cr-Cu-Fe. Calculated temperature-composition section at 40 at.% Cr

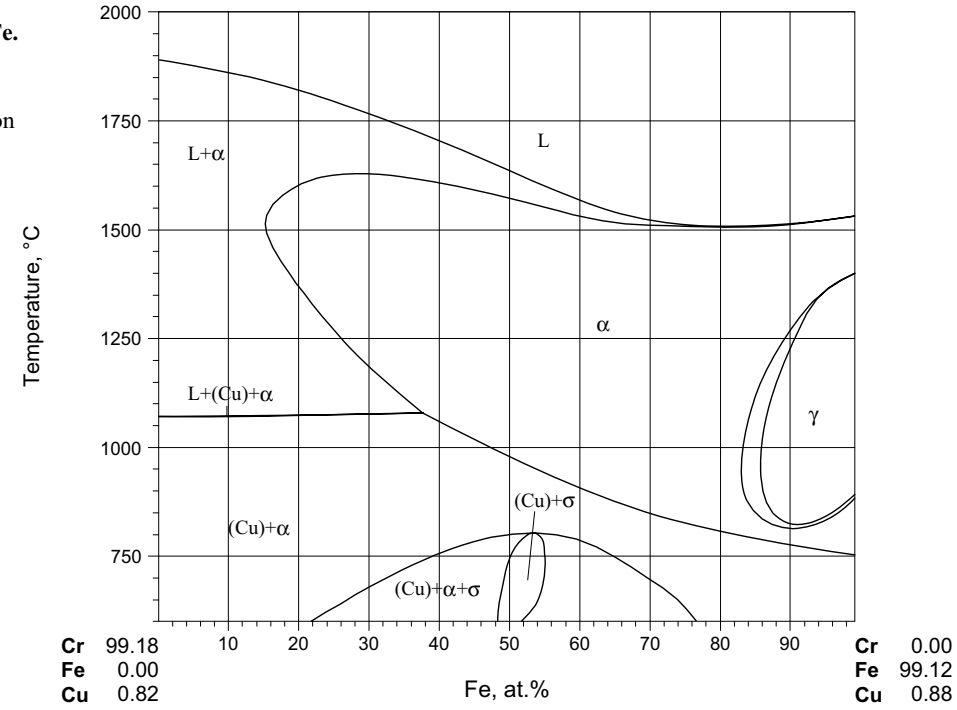

Fig. 18: Cr-Cu-Fe. Calculated temperature-composition section at 1 mass% Cu, plotted in at.%

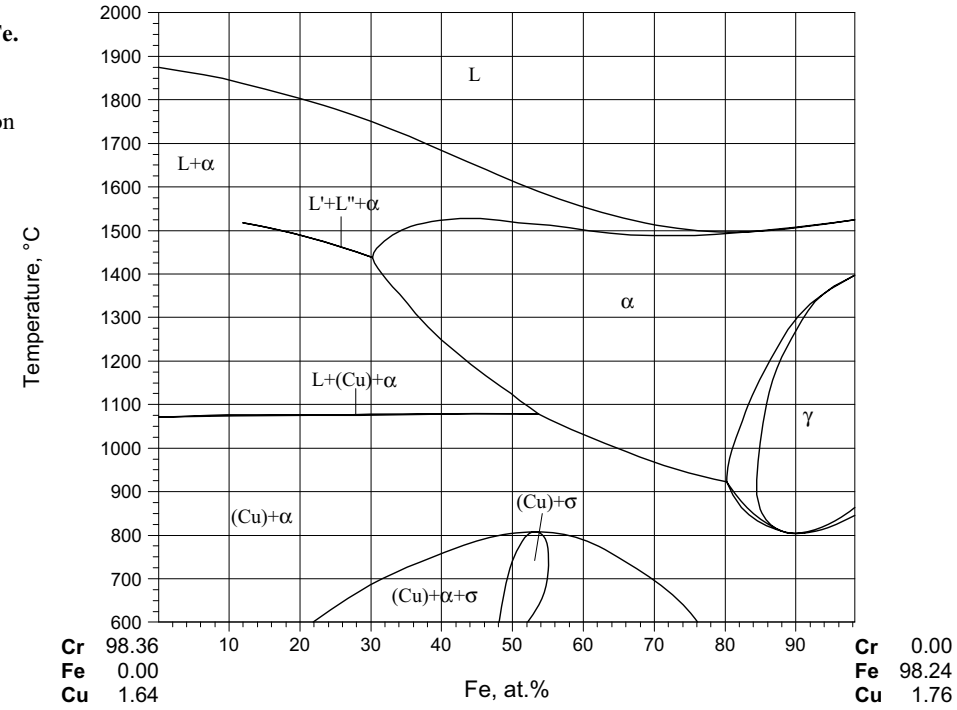

Fig. 19a: Cr-Cu-Fe. Calculated temperature-composition section at 2 mass% Cu, plotted in at.%

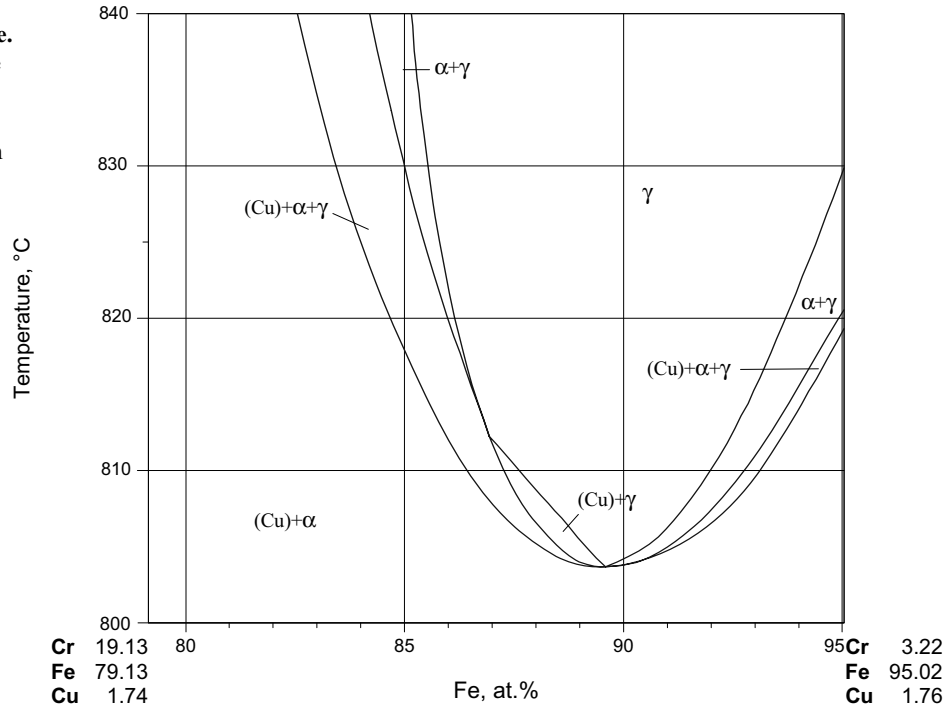

Fig. 19b: Cr-Cu-Fe. Enlarged part of the calculated temperature-composition section at 2 mass% Cu, plotted in at.%

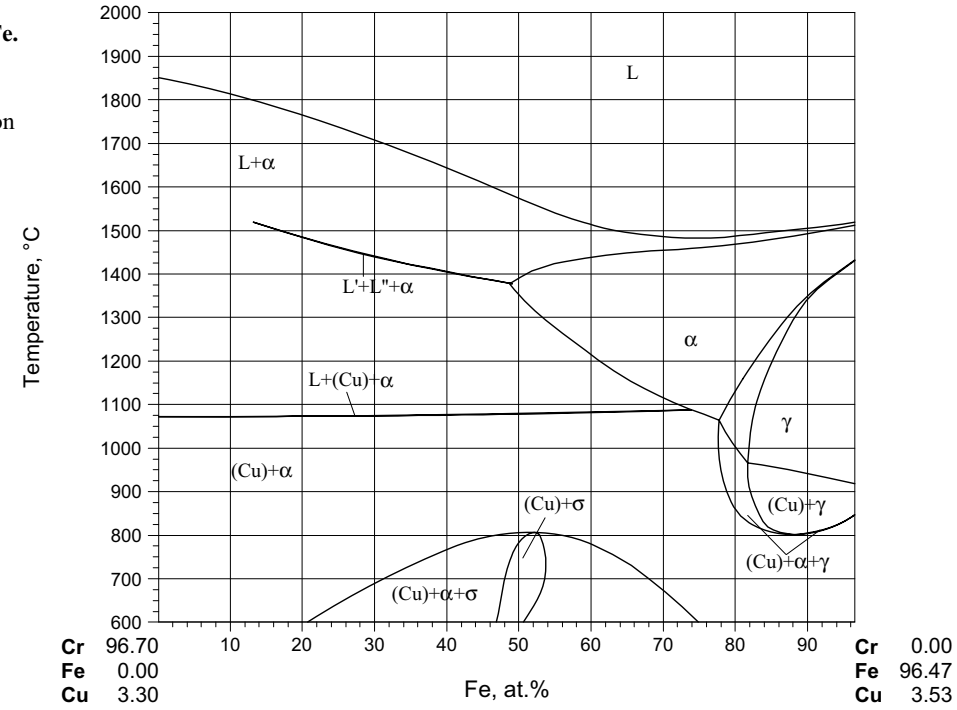

Fig. 20: Cr-Cu-Fe. Calculated temperature-composition section at 4 mass% Cu, plotted in at.%

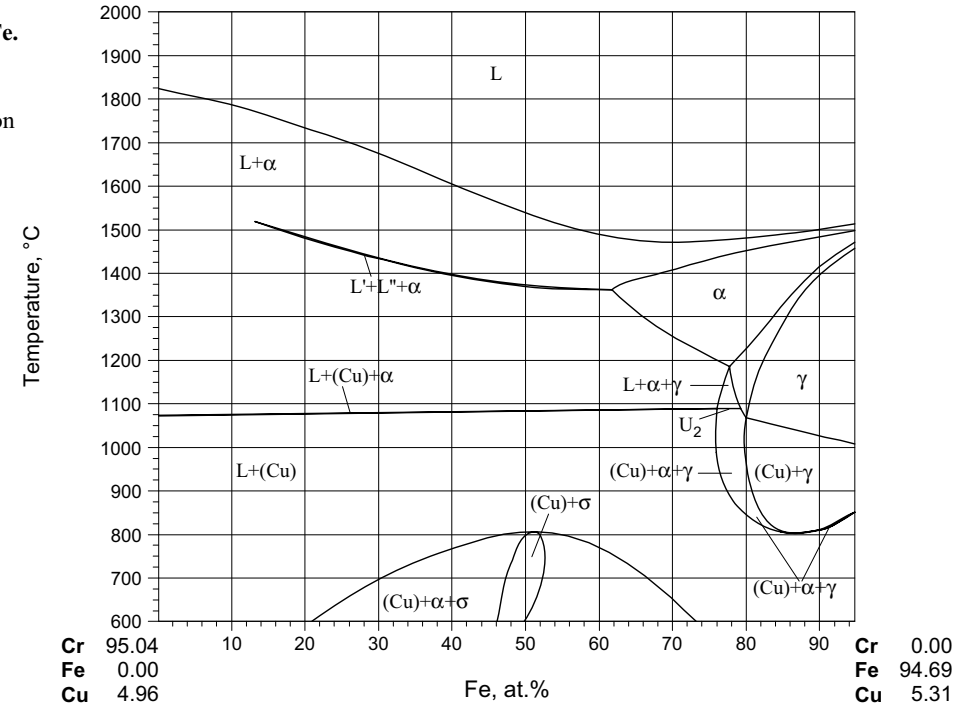

Fig. 21: Cr-Cu-Fe. Calculated temperature-composition section at 6 mass% Cu, plotted in at.%

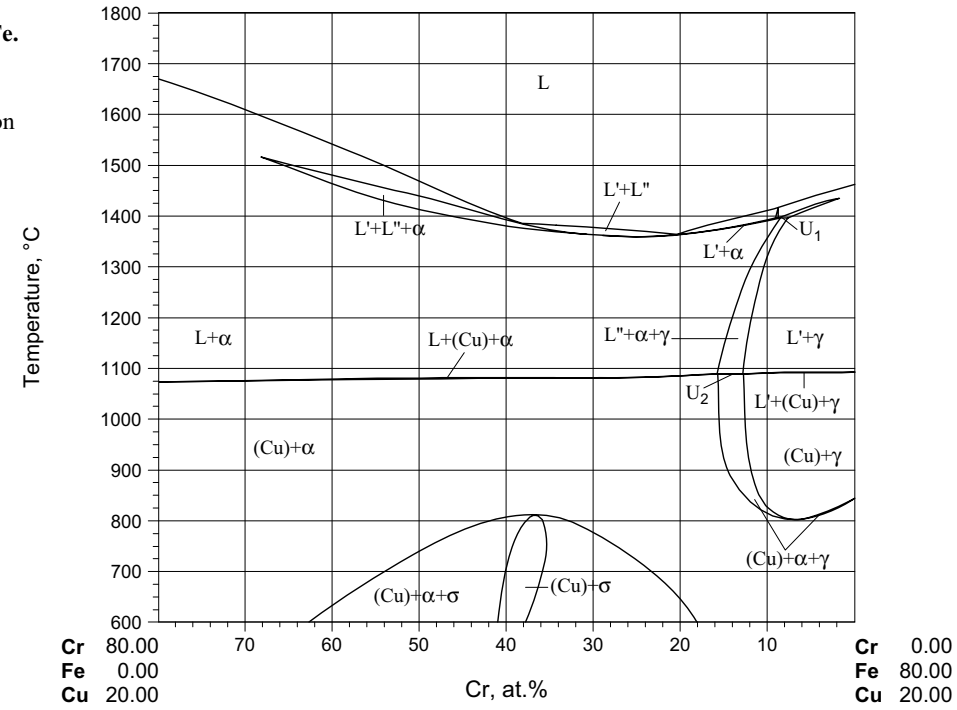

Fig. 22a: Cr-Cu-Fe. Calculated temperature-composition section at 20 at.% Cu

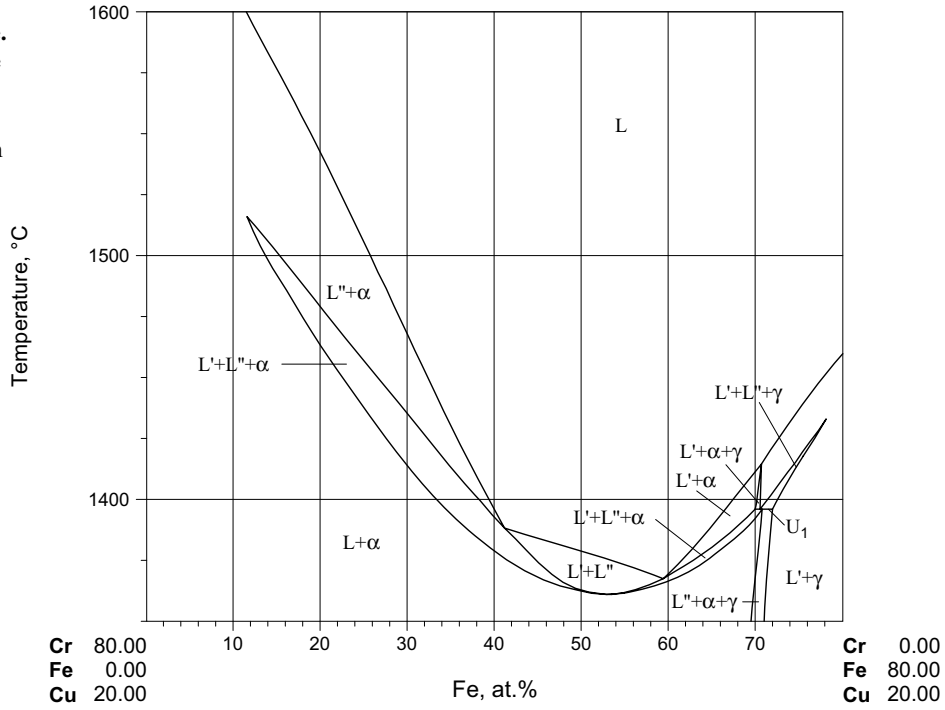

Fig. 22b: Cr-Cu-Fe. Enlarged part of the calculated temperature-composition section at 20 at.% Cu

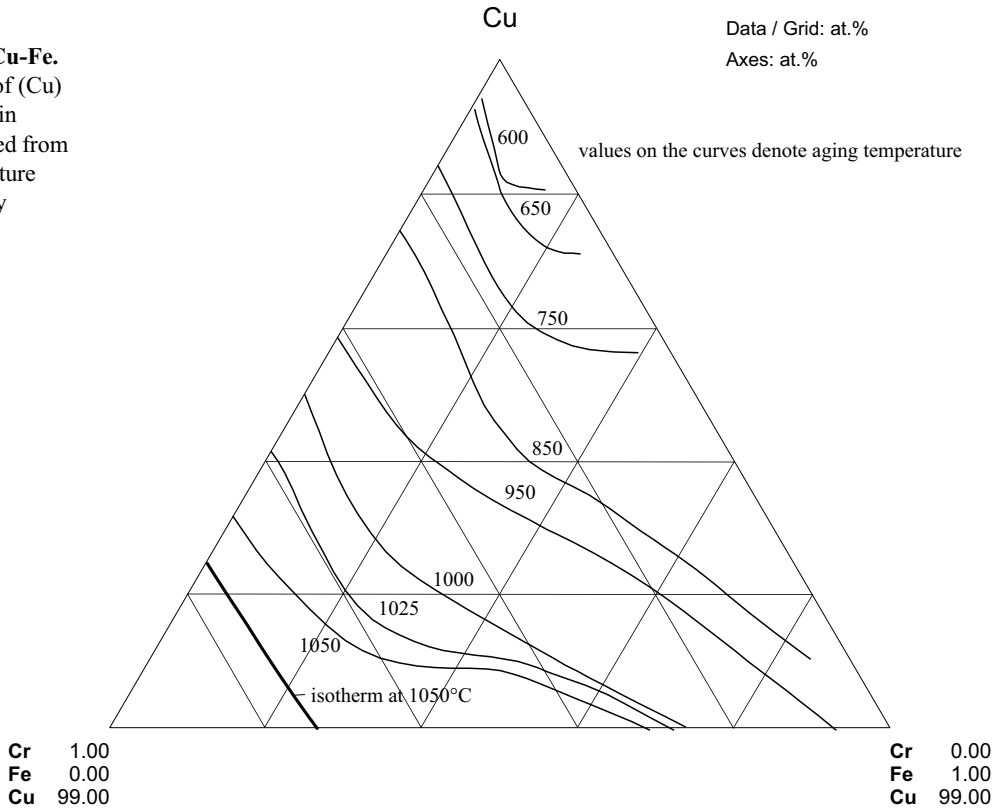

Fig. 23: Cr-Cu-Fe. Composition of (Cu) solid solution in alloys quenched from aging temperature after resistivity measurements [2001Fer1]

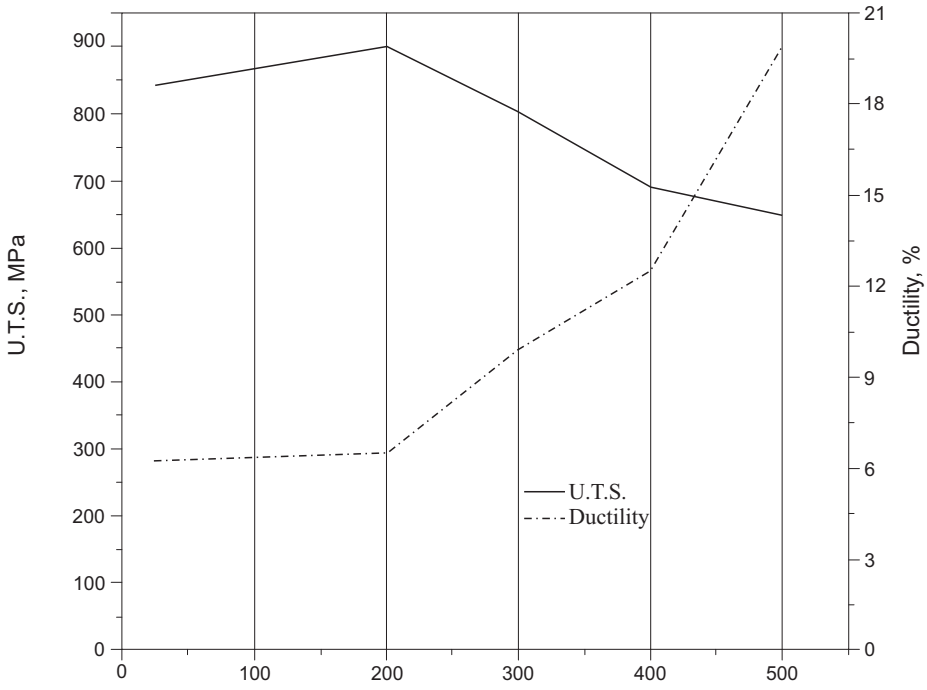

Fig. 24: Cr-Cu-Fe. Variations of ultimate tensile strength (U.T.S.) and ductility of Cu 1.2 mass% Cr 9 mass% Fe wires as a function of heat treatment temperature [2002Kim]